石炭のクリーン化に関する研究
-酸化脱硫ならびに水銀の溶出-

Study on Coal Cleaning
– Oxidative Desulfurization and Elution of Mercury –

2022

Dorcas L. E. Uaciquete

Contents

Chapter 1: Introduction

1.1 Coal utilization and coal cleaning technologies

Coal is an abundant resource with globally widespread reserves. Therefore, it has excellent supply stability and is a relatively cheaper energy source compared to other fossil fuels. Coal has been used as a major fuel source globally for centuries throughout the world, and according to predictions, this trend will continue for many years, especially in developing countries that strive to improve their standard of living. The U.S. Energy Information Administration (EIA) projected a 44% increase in world energy consumption between 2006 and 2030. In 2018, coal accounted for approximately 27% of the total world energy consumption, especially due to economic development and population growth in developing nations.

However, in recent years, the coal industry has been facing massive drawbacks because of growing environmental concerns that are mainly related to global warming caused by CO_2 emissions and the release of harmful elements. The release of sulfur, nitrogen, and mercury (Hg) is responsible for severe environmental issues such as air pollution and acid rains. Table 1.1 shows the summary of public health and environmental harms associated with coal utilization. To promote a clean environment while maintaining efficient energy generation from coal, clean coal technologies such as integrated gasification combined cycle (IGCC) and integrated gasification fuel cell (IGFC), which include high efficiency gasification and combustion and carbon capture and storage (CCS), are being developed globally.

To promote the removal of nitrogen oxides (NO_x), sulfur oxides (SO_x), particulate matter (PM), and trace elements (mainly Hg), in developed countries, a high efficiency pollutant removal technology is adopted to treat flue gas after combustion. This technology includes a denitrification unit, an electrostatic collector, and a desulfurization unit that uses limestone to achieve a high level of removal efficiency.

In the denitrification unit, NO_x are reduced using selective catalytic reduction (SCR). SCR uses a reducing agent (usually ammonia) to selectively convert NO_x from the flue gas into nitrogen gas at a certain temperature range (Fu et al., 2020).

After NO_x is removed, the exhaust gas passes through electrostatic precipitators (EPs). Here, electrical forces move particles from the air stream to the collection plates. Particles passing through the EP are given a negative electrical charge by corona action. Generally, EPs can achieve up to 99% collection efficiency for particles ranging from 1 to 10 μm (Kumar & Kumar, 2018; Miller, 2005; Santoleri, 2003; Vallero, 2019) cement substitute (Alterary & Marei, 2021; McCarthy & Dyer, 2019), but it can also contain trace levels of heavy metals such as mercury.

Before the exhaust gases are released into the atmosphere, SO_2 and SO_3 are removed by spraying limestone slurry in the desulfurization unit. Calcium carbonate in the limestone reacts with SO_2 and O_2 from the air to produce gypsum. The precipitated gypsum is recovered and further utilized in agriculture and the construction industry. The utilization of desulfurization gypsum, which was 50% in 2017, is expected to increase incrementally over the next decade (Butalia et al., 2017).

Flue gas desulfurization (FGD) technologies can result in the co-removal of 80-90% of highly-soluble oxidized mercury (Hg^{2+}), but they do not remove elemental mercury (Hg^0) (Pavlish et al., 2003). Depending on the FGD process, a portion of Hg may be incorporated into the FGD slurry and its solid byproducts including gypsum (Kairies et al., 2006).

As the multipurpose utilization of coal combustion byproducts (fly ash and FGD gypsum) expands, so does the potential for Hg release during the manufacturing and disposal process. Therefore, it is important to understand the chemical reactions that occur during the interaction of Hg and combustion byproducts, and thus develop an optimal control method.

Table 1.1 Summary of public health and environmental harms related to coal utilization (Hendryx et al., 2020).

<table>
<tr><td rowspan="2">Consequences</td><td rowspan="2">Extraction and processing</td><td colspan="2">Use</td><td rowspan="2">Waste</td></tr>
<tr><td>Power generation</td><td>Household</td></tr>
<tr><td>Public health</td><td>Respiratory illness, cancer, cardiovascular disease, kidney disease, mental health problems, mortality</td><td>Respiratory illness, cancer, cardiovascular disease, adult and infant mortality</td><td>Fluorosis, arsenism, selenosis, lung cancer, adverse child development</td><td>Child development</td></tr>
<tr><td rowspan="2">Environmental</td><td>Air, soil, and surface water and groundwater pollution, by elevated PM, ambient silica and PAHs</td><td>Air pollution through NOx, SO_2, PM, PAHs, metals emissions</td><td>Air pollution</td><td>Soil and water contamination with heavy metals, radioactive elements, PAHs</td></tr>
<tr><td colspan="4">Climate change</td></tr>
</table>

1.2 Coal Cleaning Technologies: Integrated coal Gasification Combined Cycle

Clean energy has been a major area of interest worldwide as efforts to limit greenhouse gas emissions and reduce the impact of global warming have been made. Development of IGCC is among the important advances in this area. IGCC combines two state-of-the-art technologies, (gasification and combined cycle generation); among the technologies currently available, these have the best fuel/electricity efficiency. Therefore, IGCC systems are considered a valid alternative to conventional pulverized coal plants for future power generation systems (Minchener, 2005). An IGCC typically consists of a gasification system, heat exchangers for syngas cooling, a station for fuel gas clean-up, two power blocks with gas and steam turbines, and a conversion process, which requires less energy for CO_2 removal than conventional thermal power plants.

Gasification is the process of converting various carbon-based feedstocks (coal, heavy refinery residues, petroleum coke, biomass, etc.) into syngas (Giuffrida et al., 2013). In IGCC, the feedstock is partially combusted with oxidants at high temperature and pressure; hence, the syngas is a mixture of carbon monoxide and hydrogen along with some minor components (carbon dioxide, water, hydrogen sulfide, ammonia) (Fletcher, 2017; Gray, 2017; Wang, 2017). IGCC plants can be built with net electrical efficiencies in the range of 42–46% and have considerable potential for further technological development (Cormos, 2012). Figure 1.1 shows a simplified scheme of an IGCC plant in Japan, where the gasifier uses air-blown technology, essentially relying on a reaction between coal and air to generate the combustible syngas with a net thermal efficiency of 48% on a lower heating value (LHV) basis.

Besides the suitability of IGCC as an addition to CCS systems, it offers other advantages such as low emissions of sulfur and Hg compounds and greater flexibility in process inputs and products. For gas cleaning in IGCC, raw hot syngas (at about 1500 °C) produced in the gasifier is passed through a high temperature filter system, which removes fine dust particles to meet acceptable levels set by gas turbine specifications (Jaeger, 2007). After dust removal, the syngas is further cooled to near ambient temperatures in a gas-to-gas heat exchanger. The fully cooled syngas is then passed through an acid gas removal system that washes syngas to remove sulfur and trace elements (Pisupati & Krishnamoorthy, 2017). Jaeger (2007) further explains that the removed sulfur in the form of hydrogen sulfide (H_2S) is sent to the conversion/recovery unit, where it is oxidized and absorbed in the high-performance limestone-gypsum unit. The cooled, cleaned, and desulfurized syngas is then reheated in the gas-to-gas heat exchanger

against the raw fuel gas and delivered to the gas turbine fuel control valve and specially designed low-Btu gas fuel nozzles. Despite these advantages, IGCC plants have critical obstacles to their commercialization, including the high cost of the technology, low reliability, long construction time, and lack of operating experience.

Another concern is the proper clean-up of the coal-derived syngas, which is difficult due to the inadequate temperature resistance (above 260 °C) of conventional filters (Dou et al., 2012). The current syngas clean-up technologies consist of near-ambient temperature wet-scrubbing, which contributes to a lowering of thermal efficiency. Recent studies point out that coal-derived syngas clean-up at high temperatures would be preferred to further improve the actual thermal efficiency and reduce the equipment load for syngas cooling and reheating (Giuffrida et al., 2013; Ohtsuka et al., 2009; Park et al., 2012). While hot syngas clean-up technologies are very complex, available current research, although unsuccessful, provides examples of the application and testing of these technologies. For high-temperature sulfur removal, researchers have investigated the use of metal oxides as potential sorbents. Some metal oxides, particularly zinc oxides, appeared to be suitable for the sulfidation reaction that results in sulfur removal from syngas. Since zinc tends to be reduced to its metallic state at high temperatures, which results in loss of capacity and activity via volatilization of reactive surfaces, the desulfurization temperature is limited to less than 550 °C in some cases (Giuffrida et al., 2013). In long-term tests of many successive sulfidation-regeneration cycles, the efficiency and mechanical strength of the sorbent fall to unacceptably low values (Dou et al., 2012). Therefore, coal desulfurization prior to conversion is crucial to improving power efficiency and reducing the operative cost of these systems.

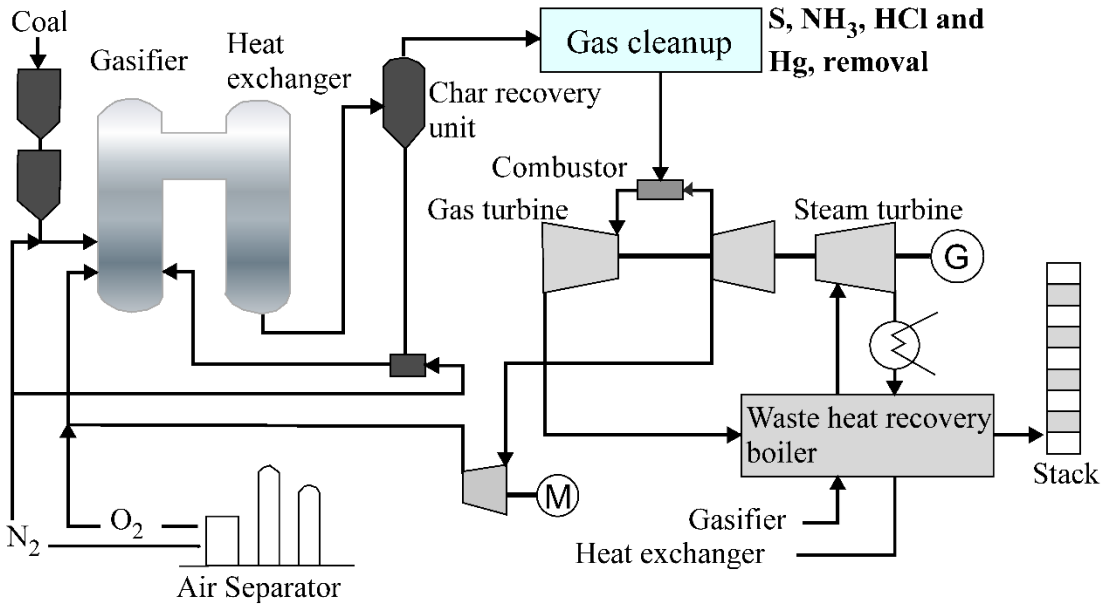

Figure 1.1 Simplified scheme of an IGCC plant showing key system components (without CCS). Source: https://i.wnp.pl/d/24/12/14/241214_940.jpg

1.3 Coal desulfurization prior to combustion

The removal of sulfur from coal prior to utilization is crucial for meeting stringent environmental regulations and the quality standards of commercial coal. Despite the well-developed technologies of exhaust gas treatment that are generally applied in IGCC plants, many reports consider that desulfurization of coal prior to combustion is the most effective and economic method for ensuring clean and environmentally friendly use of coal (Pietrzak et al., 2007; Pietrzak & Wachowska, 2006; Xia & Xie, 2017).

Sulfur in coal occurs in two main forms: organic sulfur and inorganic sulfur. Inorganic sulfur is mostly found in pyritic and sulfate forms, while organic sulfur is mainly in sulfone and thiophene forms. Inorganic sulfur such as pyrite is fairly easy to remove using flotation, magnetic separation, bio-desulfurization, pyrolysis (Hu et al., 2004; Katsuyasu Sugawara, 2001; Sahinoglu, 2018; Sugawara Katsuyasu, 2001; Uslu & Atalay, 2004; Wang et al., 2020; Ye et al., 2018; Zhang et al., 2015; Zhang et al., 2020), and selective oxidation (Borah et al., 2001, 2005; Kato, 2018; Palmer et al., 1994, 1995; Pietrzak & Wachowska, 2006; Xia & Xie, 2017). However, separation of organic sulfur is difficult using conventional methods.

The oxidative desulfurization method changes the forms of sulfur in coal and hence is considered effective for removing both organic and inorganic sulfur. One of the most effective

oxidants reported is hydrogen peroxide (H_2O_2). Mukherjee et al. (2001) found that 25% H_2O_2 alone leads to the removal of 76% pyritic sulfur, 70% sulfate sulfur, and around 5% organic sulfur. The rate of oxidation increases significantly with the increase in temperature and H_2O_2 concentration (Mukherjee et al., 2001).

Gürü et al. (2008) successfully reached a desulfurization efficiency of 74% for 12 h of reaction time by using a 15% H_2O_2 solution (Gürü et al., 2008). When using a combination of H_2O_2 and formic acid (HCOOH), 84% of inorganic sulfur and 28% of organic sulfur were removed (Baruah & Khare, 2007). However, oxidative desulfurization has major limitations. For example, to maximize organic sulfur removal, multiple reactions and high reaction temperatures are necessary. Extensive acid treatment can destroy coal properties and promote the deposition of chemical substances on coal (Borah et al., 2001), thus leading to carbon loss, particularly for low-rank coals. Therefore, in this context, the actual challenge is to remove organic sulfur without losing the raw coal properties.

1.4 Mercury control and partitioning during coal combustion

When coal burns, in addition to SO_x and NO_x, harmful trace elements such as Hg, arsenic, selenium, and zinc are also released. Hg in coal exists as a compound of sulfur and chlorine, with a content of approximately 0.1 ppm (Rallo et al., 2012). According to the U.S. Environmental Protection Agency (EPA), coal electric generating units are currently the dominant emitters of Hg, accounting for 44% of all anthropogenic emissions (Agency, 2018). In the coal combustion process, Hg moves to the gas phase through pyrolysis and combustion. When the combustion temperature of the pulverized coal boiler reaches 1500 °C, Hg is released into the exhaust gas in its elemental form (Hg^0, Hg^{2+}, or Hg_{-p}). The release of Hg and its chemical species from coal-fired power plants into the atmosphere is of major concern, owing to their strong impact on the health and ecosystems of the local people as well as the distance they travel. It is known that Hg causes various neurologic diseases, damages the immune system and kidneys, and poses a threat to the nervous system development in fetuses and newborn babies (Counter & Buchanan, 2004; Hogberg et al., 2010; Holmes et al., 2009; Mutter et al., 2004). Therefore, Hg is considered a global hazardous substance for environmental health by the EPA. To reduce Hg emissions, the EPA issued a Clean Air Mercury Rule (CAMR) in 2005.

It is known that coal-fired power plants are equipped with air pollution control devices (APCDs), which function as exhaust gas treatment equipment. Although these are not devices

whose main purpose is to remove Hg, they contribute to the suppression of Hg emissions into the atmosphere. In SCR, Hg^0 generated by coal combustion and released into the exhaust gas is oxidized to Hg^{2+} and mercury (II) chloride ($HgCl_2$) via gas-gas or gas-solid reactions (Pavlish et al., 2003; Staudt, 2006). This oxidized and low-volatile Hg is attached or adsorbed to ash particles and recovered with fly ash by using EP; consequently, the concentration of Hg increases due to a decrease in flue gas temperature and particle size (Hower et al., 2009; James C. Hower, 2000; Swanson et al., 2013). Furthermore, the remaining gaseous or ash adhered Hg^{2+} is absorbed in the solution of wet flue gas desulfurization (WFGD), distributed to desulfurization gypsum and wastewater, and discharged. Pavlish et al, (2003) reported that EP and WFGD systems installed in the U.S. remove nearly 85% and 90% of Hg_{-p} and Hg^{2+}, respectively. However, it is known that a portion of the Hg^{2+} absorbed in the WFGD can be converted back to Hg^0 and reemitted (Staudt, 2006).

Since fly ash and FGD gypsum are commonly utilized in the construction industry, there is a possibility of mobilizing the captured Hg during the manufacturing process, which would result in secondary atmospheric pollution. In addition, Hg present in coal combustion by-products that are used in concrete or landfills could leach into groundwater due to the high solubility of Hg^{2+} (Sun et al., 2014; Sun et al., 2012; Sun et al., 2015).

1.5 Aim and objectives of this study

The present study focused on coal cleaning technologies as well as the efficient utilization of coal combustion by-products. Since coal desulfurization prior to combustion is one of the crucial steps to ensure quality and reduce the risk of environmental pollution, desulfurization of raw coal was attempted through liquid-phase oxidation. Although coal-fired power plants are equipped with exhaust gas treatment units that contribute to the suppression of harmful elements, they are ineffective in removing Hg, resulting in Hg residuals within FGD gypsum and fly ash. Both FGD gypsum and fly ash have been used in cement and concrete additives, thus functioning as a good alternative to landfill materials; this has raised concerns regarding the re-release of Hg through exposure to rainwater. To accurately understand the possibility of Hg re-release from these by-products, the relationship between the chemical forms of Hg and elution behavior was investigated.

In chapter 2, to develop a desulfurization process that can be performed under mild conditions with high carbon yield, hydrogen peroxide and peracetic acid were used for selective oxidation

of subbituminous coals. The effectiveness of oxidative desulfurization was evaluated based on changes in the chemical forms of sulfur and the carbon content. Sulfur forms in the raw and treated coals were accurately specified by using Sulfur K-edge X-ray absorption near edge structure analysis (XANES). It was confirmed that inorganic sulfur (FeS_2) and some variants of sulfate were easily removed via acid leaching. Thiophenic sulfur, which is well known for being difficult to remove, was successfully converted selectively into sulfone form, which was further removed using pyrolysis without any significant carbon loss.

In chapter 3, to understand the relationship between the forms of Hg and the unburned carbon contained in fly ash, the Hg forms in fly ash with a rich fraction of unburned carbon were qualitatively and quantitatively analyzed via Hg L_{III}-edge XANES analysis. Estimation of chemical forms of Hg was initially performed using an inflection point method. Using the first derivatives of the XANES spectra, the inflection point difference was calculated as the difference between two maximum points of absorption energy with the zero points of the second derivative. Subsequently, Hg forms were estimated by comparing ΔE samples to control compounds. Additionally, qualitative and quantitative analyses of the control Hg compounds were performed via linear combination fitting using XANES spectra. The XANES spectrum of the unburned carbon samples showed that the entire Hg content is bound to sulfur, chlorine, and oxygen compounds. Furthermore, it was demonstrated that the Hg content depends on the unburned carbon and sulfur contents.

In chapter 4, to clarify the re-release behavior of Hg from coal combustion by-products, we attempted to develop an accurate method for evaluating Hg elution from desulfurization gypsum. The relationship between Hg chemical forms and elution behavior was explained. This was achieved by conducting elution tests in a batch system according to the environmental standards by using a semi-batch system developed in this study. Total Hg contents in the solutions were determined using cold vapor atomic adsorption spectroscopy (CVAAS), and the change in Hg chemical forms in residues was analyzed via a combination of temperature programmed desorption and cold vapor atomic adsorption spectroscopy (TPD-CVAAS). When using the batch system, a sequential phenomenon of elution and adsorption of Hg was observed, which restricted the precise evaluation of the amount of Hg eluted. Meanwhile, when using the semi-batch system, the elution of Hg attained a constant value without the interference of

adsorption phenomena. It was concluded that both the extent of elution as well as the elution behavior are dependent mainly on the Hg content bound with carbon in the samples.

References

Agency, U. S. E. P. (2018). *2014 National Emissions Inventory, version 2 Technical Support Document*. U.S.A Retrieved from https://www.epa.gov/sites/default/files/2018-07/documents/nei2014v2_tsd_05jul2018.pdf

Alterary, S. S., & Marei, N. H. (2021). Fly ash properties, characterization, and applications: A review. *Journal of King Saud University - Science*, *33*(6), 101536. https://doi.org/10.1016/j.jksus.2021.101536

Baruah, B. P., & Khare, P. (2007). Desulfurization of Oxidized Indian Coals with Solvent Extraction and Alkali Treatment. *Energy & Fuels*, *21*(4), 2156-2164. https://doi.org/10.1021/ef070087a

Borah, D., Baruah, M. K., & Haque, I. (2001). Oxidation of high sulphur coal. Part 2. Desulphurisation of organic sulphur by hydrogen peroxide in presence of metal ions. *Fuel*, *80*(10), 1475-1488. https://doi.org/10.1016/s0016-2361(01)00002-3

Borah, D., Baruah, M. K., & Haque, I. (2005). Oxidation of high sulphur coal.9 3. Desulphurisation of organic sulphur by peroxyacetic acid (produced in situ) in presence of metal ions. *Fuel Processing Technology*, *86*(9), 959-976. https://doi.org/10.1016/j.fuproc.2004.11.015

Butalia, T., Wolfe, W., & Amaya, P. (2017). 6 - The utilization of flue-gas desulfurization materials. In T. Robl, A. Oberlink, & R. Jones (Eds.), *Coal Combustion Products (CCP's)* (pp. 155-184). Woodhead Publishing. https://doi.org/https://doi.org/10.1016/B978-0-08-100945-1.00006-X

Cormos, C.-C. (2012). Integrated assessment of IGCC power generation technology with carbon capture and storage (CCS). *Energy*, *42*(1), 434-445. https://doi.org/10.1016/j.energy.2012.03.025

Counter, S. A., & Buchanan, L. H. (2004). Mercury exposure in children: a review. *Toxicol Appl Pharmacol*, *198*(2), 209-230. https://doi.org/10.1016/j.taap.2003.11.032

Dou, B., Wang, C., Chen, H., Song, Y., Xie, B., Xu, Y., & Tan, C. (2012). Research progress of hot gas filtration, desulphurization and HCl removal in coal-derived fuel gas: A review. *Chemical Engineering Research and Design*, *90*(11), 1901-1917. https://doi.org/10.1016/j.cherd.2012.04.009

Fletcher, T. H. (2017). Gasification fundamentals. In (pp. 223-256). Elsevier. https://doi.org/10.1016/b978-0-08-100167-7.00006-8

Fu, J., Xiao, H., Wang, H., & Zhou, J. (2020). Control Strategy for Denitrification Efficiency of Coal-Fired Power Plant Based on Deep Reinforcement Learning. *IEEE Access*, *8*, 65127-65136. https://doi.org/10.1109/access.2020.2985233

Giuffrida, A., Romano, M. C., & Lozza, G. (2013). Efficiency enhancement in IGCC power plants with air-blown gasification and hot gas clean-up. *Energy*, *53*, 221-229. https://doi.org/10.1016/j.energy.2013.02.007

Gray, D. D. (2017). Major gasifiers for IGCC systems. In (pp. 305-355). Elsevier. https://doi.org/10.1016/b978-0-08-100167-7.00008-1

Gürü, M., Sariöz, B. V., & Çakanyildirim, Ç. (2008). Oxidative Desulfurization of Tufanbeyli Coal by Hydrogen Peroxide Solution. *Energy Sources, Part A: Recovery, Utilization, and Environmental Effects*, *30*(11), 981-987. https://doi.org/10.1080/00908310600714006

Hendryx, M., Zullig, K. J., & Luo, J. (2020). Impacts of Coal Use on Health. *Annu Rev Public Health*, *41*, 397-415. https://doi.org/10.1146/annurev-publhealth-040119-094104

Hogberg, H. T., Kinsner-Ovaskainen, A., Coecke, S., Hartung, T., & Bal-Price, A. K. (2010). mRNA Expression is a Relevant Tool to Identify Developmental Neurotoxicants Using an In Vitro Approach. *Toxicological Sciences*, *113*(1), 95-115. https://doi.org/10.1093/toxsci/kfp175

Holmes, P., James, K. A., & Levy, L. S. (2009). Is low-level environmental mercury exposure of concern to human health? *Sci Total Environ*, *408*(2), 171-182. https://doi.org/10.1016/j.scitotenv.2009.09.043

Hower, J. C., Robl, T. L., Thomas, G. A., Hopps, S. D., & Grider, M. (2009). Chemistry of coal and coal combustion products from Kentucky power plants: Results from the 2007 sampling, with emphasis on selenium. *Coal Combustion and Gasification Products*, *1*(1), 50-62. https://doi.org/10.4177/ccgp-d-09-00013.1

Hu, H., Zhou, Q., Zhu, S., Meyer, B., Krzack, S., & Chen, G. (2004). Product distribution and sulfur behavior in coal pyrolysis. *Fuel Processing Technology*, *85*(8-10), 849-861. https://doi.org/10.1016/j.fuproc.2003.11.030

Jaeger, H. (2007). Japan 250 MW coal based IGCC demo plant set for 2007 start-up. *Gas turbine world*.

James C. Hower, M. M. M.-V., Darrell N. Taulbee and Tanaporn Sakulpitakphon. (2000). Mercury Capture by Distinct Fly Ash Carbon Forms. *Energy & Fuels*, *14*, 224-226.

Kairies, C., Schroeder, K., & Cardone, C. (2006). Mercury in gypsum produced from flue gas desulfurization. *Fuel*, *85*(17-18), 2530-2536. https://doi.org/10.1016/j.fuel.2006.04.027

Kato, T. N., Yuki; Okawa, Hirokazu; Sugawara, Katsuyasu. (2018). Behavior of Sulfur in Liquid Phase Oxidation of Coal. *Journal of the Japan Institute of energy*, *97*, 88-96.

Katsuyasu Sugawara, Y. E., Takuo Sugawara and Masayuki Shirai. (2001). XANES analysis of sulfur form change during pyrolysis of coals. *Journal of Synchroton Radiation*, *8*, 955-957.

Kumar, D., & Kumar, D. (2018). Chapter 12 - Dust Control. In D. Kumar & D. Kumar (Eds.), *Sustainable Management of Coal Preparation* (pp. 265-278). Woodhead Publishing. https://doi.org/https://doi.org/10.1016/B978-0-12-812632-5.00012-4

McCarthy, M. J., & Dyer, T. D. (2019). Pozzolanas and pozzolanic materials. *Lea's Chemistry of Cement and Concrete*, 363-467.

Miller, B. G. (2005). CHAPTER 6 - Emissions Control Strategies for Power Plants. In B. G. Miller (Ed.), *Coal Energy Systems* (pp. 283-392). Academic Press. https://doi.org/https://doi.org/10.1016/B978-012497451-7/50006-1

Minchener, A. J. (2005). Coal gasification for advanced power generation. *Fuel*, *84*(17), 2222-2235. https://doi.org/10.1016/j.fuel.2005.08.035

Mukherjee, S., Mahiuddin, S., & Borthakur, P. C. (2001). Demineralization and Desulfurization of Subbituminous Coal with Hydrogen Peroxide. *Energy & Fuels*, *15*(6), 1418-1424. https://doi.org/10.1021/ef010061y

Mutter, J., Naumann, J., Sadaghiani, C., Walach, H., & Drasch, G. (2004). Amalgam studies: disregarding basic principles of mercury toxicity. *Int J Hyg Environ Health*, *207*(4), 391-397. https://doi.org/10.1078/1438-4639-00305

Ohtsuka, Y., Tsubouchi, N., Kikuchi, T., & Hashimoto, H. (2009). Recent progress in Japan on hot gas cleanup of hydrogen chloride, hydrogen sulfide and ammonia in coal-derived fuel gas. *Powder Technology*, *190*(3), 340-347. https://doi.org/10.1016/j.powtec.2008.08.012

Palmer, S. R., Hippo, E. J., & Dorai, X. A. (1994). Chemical coal cleaning using selective oxidation. *Fuel*, *73*(2), 161-169. https://doi.org/10.1016/0016-2361(94)90109-0

Palmer, S. R., Hippo, E. J., & Dorai, X. A. (1995). Selective oxidation pretreatments for the enhanced desulfurization of coal. *Fuel*, *74*(2), 193-200. https://doi.org/10.1016/0016-2361(95)92654-o

Park, Y. C., Jo, S.-H., Ryu, H.-J., Moon, J.-H., Yi, C.-K., Yoon, Y., & Baek, J.-I. (2012). Simultaneous removal of H2S and COS using Zn-based solid sorbents in the bench-scale continuous hot gas desulfurization system integrated with a coal gasifier. *Korean Journal of Chemical Engineering*, *29*(12), 1812-1816. https://doi.org/10.1007/s11814-012-0059-3

Pavlish, J. H., Sondreal, E. A., Mann, M. D., Olson, E. S., Galbreath, K. C., Laudal, D. L., & Benson, S. A. (2003). Status review of mercury control options for coal-fired power plants. *Fuel Processing Technology*, *82*(2-3), 89-165. https://doi.org/10.1016/s0378-3820(03)00059-6

Pietrzak, R., Grzybek, T., & Wachowska, H. (2007). XPS study of pyrite-free coals subjected to different oxidizing agents. *Fuel*, *86*(16), 2616-2624. https://doi.org/10.1016/j.fuel.2007.02.025

Pietrzak, R., & Wachowska, H. (2006). The influence of oxidation with HNO3 on the surface composition of high-sulphur coals: XPS study. *Fuel Processing Technology*, *87*(11), 1021-1029. https://doi.org/10.1016/j.fuproc.2006.08.001

Pisupati, S. V., & Krishnamoorthy, V. (2017). Utilization of coal in IGCC systems. In *Integrated Gasification Combined Cycle (IGCC) Technologies* (pp. 83-120). https://doi.org/10.1016/b978-0-08-100167-7.00002-0

Rallo, M., Heidel, B., Brechtel, K., & Maroto-Valer, M. M. (2012). Effect of SCR operation variables on mercury speciation. *Chemical Engineering Journal*, *198-199*, 87-94. https://doi.org/10.1016/j.cej.2012.05.080

Sahinoglu, E. (2018). Cleaning of high pyritic sulfur fine coal via flotation. *Advanced Powder Technology*, *29*(7), 1703-1712. https://doi.org/10.1016/j.apt.2018.04.005

Santoleri, J. J. (2003). Hazardous Waste Incineration. In R. A. Meyers (Ed.), *Encyclopedia of Physical Science and Technology (Third Edition)* (pp. 223-244). Academic Press. https://doi.org/https://doi.org/10.1016/B0-12-227410-5/00308-2

Staudt, R. K. S. N. H. B. M. F. P. J. (2006). An overview of the status of mercury control technologies. *Environmental Scienec & Technology*, 1385-1393. https://pubs.acs.org/doi/pdf/10.1021/es062639u

Sugawara Katsuyasu, E. Y., Sugawara Takuo, Shirai Masayuki. (2001). XANES analysis of sulfur form change during pyrolysis of coals. *Journal of Synchroton Radiation*, *8*, 955-957.

Sun, M., Cheng, G., Lu, R., Tang, T., Baig, S. A., & Xu, X. (2014). Characterization of Hg0 re-emission and Hg2+ leaching potential from flue gas desulfurization (FGD) gypsum. *Fuel Processing Technology*, *118*, 28-33. https://doi.org/10.1016/j.fuproc.2013.08.002

Sun, M., Hou, J., Tang, T., Lu, R., Cheng, L., & Xu, X. (2012). Stabilization of mercury in flue gas desulfurization gypsum from coal-fired electric power plants with additives. *Fuel Processing Technology*, *104*, 160-166. https://doi.org/10.1016/j.fuproc.2012.05.008

Sun, M., Lou, Z., Cheng, G., Baig, S. A., Fang, L., Zhou, X., Shen, Y., & Xu, X. (2015). Process migration and transformation of mercury in simulated wet flue gas desulfurization slurry system. *Fuel*, *140*, 136-142. https://doi.org/10.1016/j.fuel.2014.09.094

Swanson, S. M., Engle, M. A., Ruppert, L. F., Affolter, R. H., & Jones, K. B. (2013). Partitioning of selected trace elements in coal combustion products from two coal-burning power plants in the United States. *International Journal of Coal Geology*, *113*, 116-126. https://doi.org/10.1016/j.coal.2012.08.010

Uslu, T., & Atalay, Ü. (2004). Microwave heating of coal for enhanced magnetic removal of pyrite. *Fuel Processing Technology*, *85*(1), 21-29. https://doi.org/10.1016/s0378-3820(03)00094-8

Vallero, D. A. (2019). Air pollution control technologies. In (pp. 377-428). Elsevier. https://doi.org/10.1016/b978-0-12-814934-8.00013-2

Wang, M., Shen, Y., Hu, Y., Kong, J., Wang, J., & Chang, L. (2020). Effect of pre-desulfurization process on the sulfur forms and their transformations during pyrolysis of Yanzhou high sulfur coal. *Fuel*, *276*, 118124. https://doi.org/10.1016/j.fuel.2020.118124

Wang, T. (2017). An overview of IGCC systems. In (pp. 1-80). Elsevier. https://doi.org/10.1016/b978-0-08-100167-7.00001-9

Xia, W., & Xie, G. (2017). A technological review of developments in chemical-related desulfurization of coal in the past decade. *International Journal of Mineral Processing*, *161*, 65-71. https://doi.org/10.1016/j.minpro.2017.02.013

Ye, J., Zhang, P., Zhang, G., Wang, S., Nabi, M., Zhang, Q., & Zhang, H. (2018). Biodesulfurization of high sulfur fat coal with indigenous and exotic microorganisms. *Journal of Cleaner Production*, *197*, 562-570. https://doi.org/10.1016/j.jclepro.2018.06.223

Zhang, B., Zhao, Y., Zhou, C., Duan, C., & Dong, L. (2015). Fine Coal Desulfurization by Magnetic Separation and the Behavior of Sulfur Component Response in Microwave

Energy Pretreatment. *Energy & Fuels*, *29*(2), 1243-1248. https://doi.org/10.1021/ef502003g

Zhang, Z., Yan, G., Zhu, G., Zhao, P., Ma, Z., & Zhang, B. (2020). Using microwave pretreatment to improve the high-gradient magnetic-separation desulfurization of pulverized coal before combustion. *Fuel*, *274*. https://doi.org/10.1016/j.fuel.2020.117826

Chapter 2: Coal desulfurization by oxidative treatment

2.1. Introduction

Coal is used not only for electricity generation, but it is also a very important source in steel making process. In the steel industry particularly requires large quantities of bituminous coal to produce coke and subbituminous coal as a heat source in converter furnaces. Due to increasingly growing in the world`s energy consumption, reserves of high rank coal with low sulfur, low ash and high calorific value are rapidly depleting (De Filippis et al., 2010; Dong, 2011). Therefore, it is essential to develop technologies for the removal of sulfur from high rank coals and assure the use of these coals in steelmaking.

Coal desulfurization can be conducted by tree main methods: (1) Physical, (2) biological and (3) biological methods.

Physical methods utilize differences in density and surface properties between mineral and organic materials and are particularly effective in removing inorganic sulfur such as pyrite and soluble sulphates (Ambedkar et al., 2011; Sönmez & Giray, 2001), but it does not remove fine pyrite and organic-bound sulfur. Biological methods are mild treatments at room temperature and can remove both organic and inorganic sulfur without carbon loss (Acharya et al., 2001; Aller et al., 2001; Gonsalvesh et al., 2013; Handayani et al., 2017; Martínez et al., 2017; Mohebali et al., 2007; Singh et al., 2013), but have the disadvantages of extremely long incubation time and the inconsistency in desulfurization characteristics (Çelik et al., 2019; Kotelnikov et al., 2020; Rossi, 2014). On the other hand, chemical desulfurization is an effective method for removing inorganic and organic sulfur. Several reports demonstrate that fine pyrite and sulfate sulfur that cannot be physically removed can be removed by chemical treatment (Ali et al., 1992; Mukherjee & Borthakur, 2001; Mukherjee & Borthakur, 2003; Mukherjee & Borthakur, 2004; Ratanakandilok et al., 2001). However, the removal rate of organic sulfur especially thiophene sulfur is low with these methods. In addition, thiophene sulfur in high rank coals with high degree of carbonization is particularly difficult to oxidize under mild conditions (George et al., 1991; Kato et al., 2018). Furthermore, the low carbon yield is a consistent problem when chemical desulfurization is carried out.

Treatment with strong oxidants such as potassium $KMnO_4$ is found to be effective to oxidize pyrite and organic sulfur into soluble sulfate forms, however, the treated coal shows an increase in the ash content ana a significant loss of calorific value (Ghauri et al., 2016).

Hydrogen peroxide (H_2O_2) on the other hand, which decomposes into H_2O and O_2 after the reaction and leaves no chemical residues in the coal, is attracting attention as a desulfurization agent. However, it has been shown that H_2O_2 is less effective for thiophene sulfur removal

especially in high rank coals (Kato et al., 2018; Mukherjee et al., 2001). The oxidation of thiophene sulfur in diesel oil using organic peroxides, which are reaction products of hydrogen peroxide and organic acids have been reported (De Filippis et al., 2011; De Filippis et al., 2010; Yazu Kazumasa, 2010). Reports show that thiophene sulfur is oxidized to sulfoxide and then converted into sulfone-sulfur which can be removed by extraction with polar solvents. However, there is limited information on this process in coal. In addition, the details about the changes on sulfur morphology and the changes in carbon yield during oxidation treatment are not yet clear.

In this study, two types of Chinese subbituminous coals were oxidized using H_2O_2 and peracetic acid. The effectiveness of oxidative desulfurization was determined from the changes in sulfur morphology and carbon content. In the hydrogen peroxide treatment, the effect of the oxidation temperature was investigated. Further, the effectiveness of the thermal decomposition treatment for sulfone removal was determined.

2.2 Experimental methods

2.2.1. Coal samples

In this study, SB and NA coals, which are subbituminous coals Shaanxi and Shandong, China, respectively, were crushed and sieved to -42+65 mesh and dried at 107±5 ℃ for 24 h prior to use. The average particle sizes were 299 and 285 μm for coal SB and NA, respectively. Table 2.1 shows the ultimate and proximate analyses for each sample.

Table 2.1 Ultimate and proximate analyses of samples

Sample	Ultimate [wt.%, d.a.f.]					Proximate [wt.%, d.b.]	
	C	H	N	S	O^{diff}	V.M.	Ash
SB	78.5	4.6	0.8	0.2	15.9	38.2	6.8
NA	77.1	4.9	1.5	0.5	9.3	33.2	6.7

2.2.2. Oxidative treatment

The oxidation treatment was carried out using hydrogen peroxide (H_2O_2) and peracetic acid (PAA) as oxidizing agents. The details of the procedure are shown in Figures 2.1 and 2.2. Oxidation by H_2O_2 was carried out by mixing 25 mL of 30% hydrogen peroxide solution (GR, Nacalai Tesque) and 15 mL of distilled water with 1 g of each coal sample and stirring for 2-24 h at 20-60 ℃.

In the oxidation using PAA, PAA was generated at low temperature according to equation (1).

$$(CH_3CO)_2O + H_2O_2 \rightarrow CH_3COOOH + CH_3COOH \quad (1)$$

H_2O_2 (30%; 25 mL; EP, Nacalai Tesque) and acetic anhydride (15 mL; GR, Nacalai Tesque) were mixed with 1 g of coal, and the mixture was stirred at 20 ℃ for 2-24h. As Kato (2018) described, the desulfurization of subbituminous coal does not proceed at 20 ℃, so here, the temperature was increased.

After oxidation, the sample was filtered using a cellulose mixed ester-type membrane filter (AS ONE Corporation). The residue was washed with distilled water and dried at 107 ± 5 ℃ for 24 h to obtain the oxidized sample.

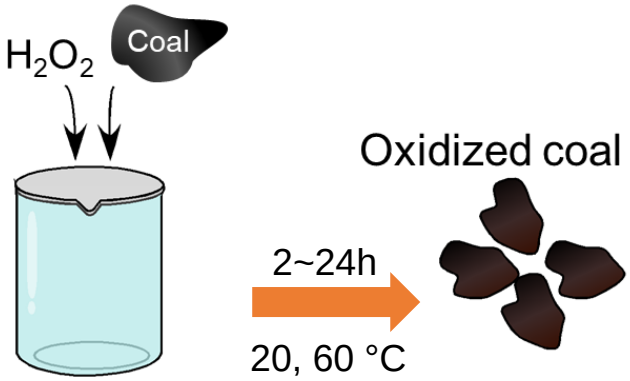

Figure 2.1 Oxidative treatment by hydrogen peroxide (H_2O_2).

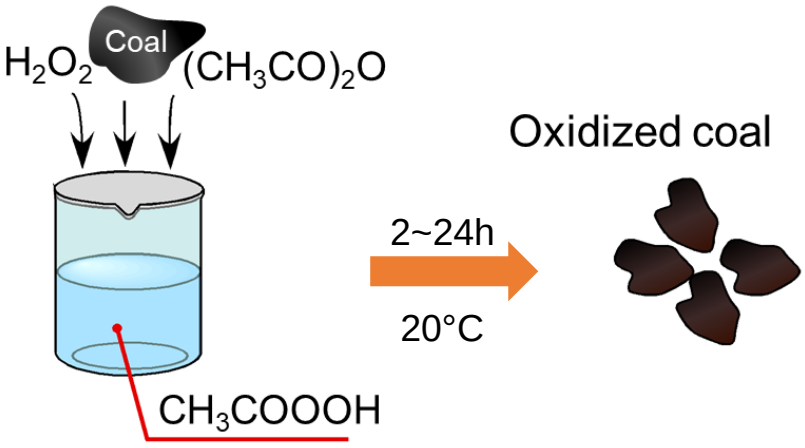

Figure 2.2 Oxidative treatment by peracetic acid (PAA).

2.2.3. Elemental and XANES analyses

Elemental analyses were conducted using a nitrogen, carbon, and hydrogen analyzer (NCH-22, Sumica Chemical Analysis Service Ltd.) and a carbon and sulfur analyzer (EMIA 220V, HORIBA Ltd.). Sulfur K-edge X-ray absorption near edge structure (XANES) were carried out using beam line 11B at the Photon Factory (High Energy Physics Laboratory, Tsukuba, Japan) with an optical system consisting of Ni-coated Si, a bent cylinder mirror, and a Si (111) double crystal monochromator. Crushed raw and oxidized samples were fixed on the sample holder with conductive tape and then placed in a vacuum chamber at 10-5 torr. The irradiated energy was calibrated using the 2481.7 eV peak of K_2SO_4 (GR, Nacalai Tesque) and the XANES spectra were obtained in the energy range of 2450−2520 eV to determine the chemical forms of sulfur in raw and oxidized coal.

Potassium sulfate, thioxane (GR, Tokyo Chemical Industry Co., Ltd.), diphenylsulfone (GR, Tokyo Chemical Industry co., Ltd.), 4,4-dinitrophenylsulfide (EP, Tokyo Chemical Industry Co., Ltd.), DL-methionine sulfoxide (EP, Tokyo Chemical Industry Co., Ltd.), and pyrite were used as model compounds.

The sulfur forms were quantitatively analyzed using the XANES spectra of the model compounds as described by Huffman et al. (1991). A calibration curve was prepared from the relationship between the ratio of the peak areas determined from the fluorescence spectrum and the ratio of the sulfur contents of thiophene and other sulfur compounds. The peak areas of various sulfur compounds were determined by curve fitting, where a 50% Gaussian function and 50% Lorentzian function was used to represent each sulfur compound. The curve fitting was carried out using the nonlinear least-squares method. The edge jumps are centered near 2475 and 2485 eV, although these values vary depending on the sample. The absorption edge (E_0) and half width at half maximum (σ) of the sulfur compounds are shown in Table 2.2.

2.2.4. Thermal treatment

Thermal treatment of oxidized samples was carried out in a horizontal fixed bed reactor as shown in Figure 2.3.

Peracetic acid treated sample at 12h was placed in a quartz boat and then inserted in a horizontal reactor (quartz tube, 492.5 mm × 24.5 mm, i.d. × length). The temperature of the reactor was controlled by a temperature programmed electric furnace. Nitrogen gas was supplied at a flow rate of 200 mL-NTP/min, and the furnace temperature was raised to 400 °C at a heating rate of

5 °C/min. The pyrolysis temperature was selected from the fact that the yield of pyrolysis char decreases when the temperature is higher than 400 °C (Sugawara et al., 1994).

Table 2.2 Fitting parameters for the sulfur K-edge XANES spectra

Sulfur form	E0	σ
FeS2	2471.5	1.5
Sulfide	2472.8	1.7
Thiophene	2473.3	1.7
Sulfoxide	2474.5–2475.5	1.7
Sulfone	2479.5–2480.0	3.5
Sulfate	2481.7	3.0

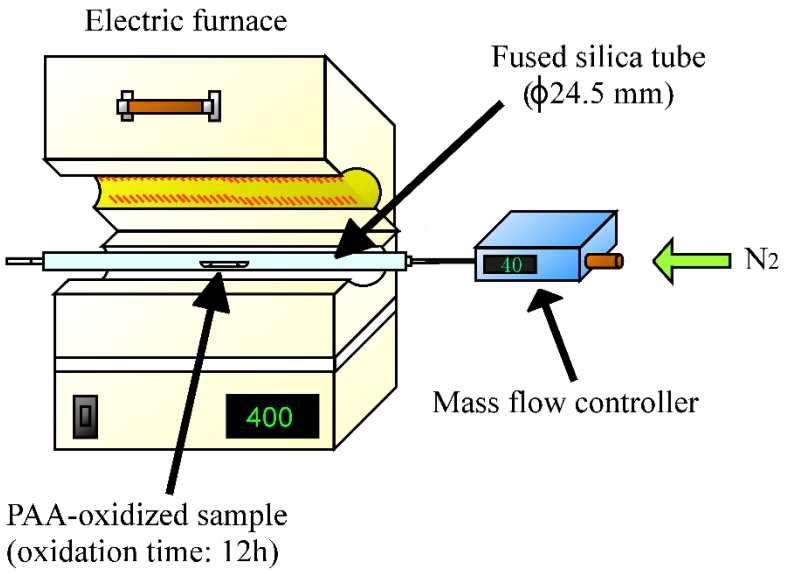

Figure 2.3 Schematic diagram of thermal treatment fixed reactor

2.3 Results and discussion

2.3.1 Sulfur forms in raw coals

Figure 2.4 shows the normalized and the respective third derivative of the sulfur K-edge XANES spectra of raw SB and NA coals. Both coals show large peaks near 2473 and 2482 eV. Third-derivative from model samples are fingerprints for interpreting sulfur forms in the samples (Sugawara Katsuyasu, 2001). For both coals, thiophene, sulfoxide and sulfate peaks were confirmed. In addition, the shoulder peak of pyrite indicates that pyrite content in raw SB coal is higher than that of NA coal. Using the least-squares method, separation of pyrite, thiophene, sulfoxide and sulfate peaks was performed as shown in Figure 2.5. And by analyzing the XANES spectra of raw SB and NA coals, it was confirmed that all organic sulfur in raw coals used are thiophenic form, and that various organic sulfur such as sulfide and sulfone are not contained in the raw samples. The peaks of thiophene (b) and sulfate (e) were observed at 2473.3 and 2481.7 eV, respectively. In coal SB, the pyrite (a) and sulfoxide (c) peaks were observed at 2471.5 and 2475.0 eV. And no peaks of sulfone (d) were observed for both coals. Table 2.3 shows the sulfur form distributions determined by peak separation of the XANES spectra. The thiophene, pyrite, and sulfate amounts in raw SB are 63%, 28%, and 9%, respectively, whereas for coal NA, 87% of sulfur is in the thiophenic form.

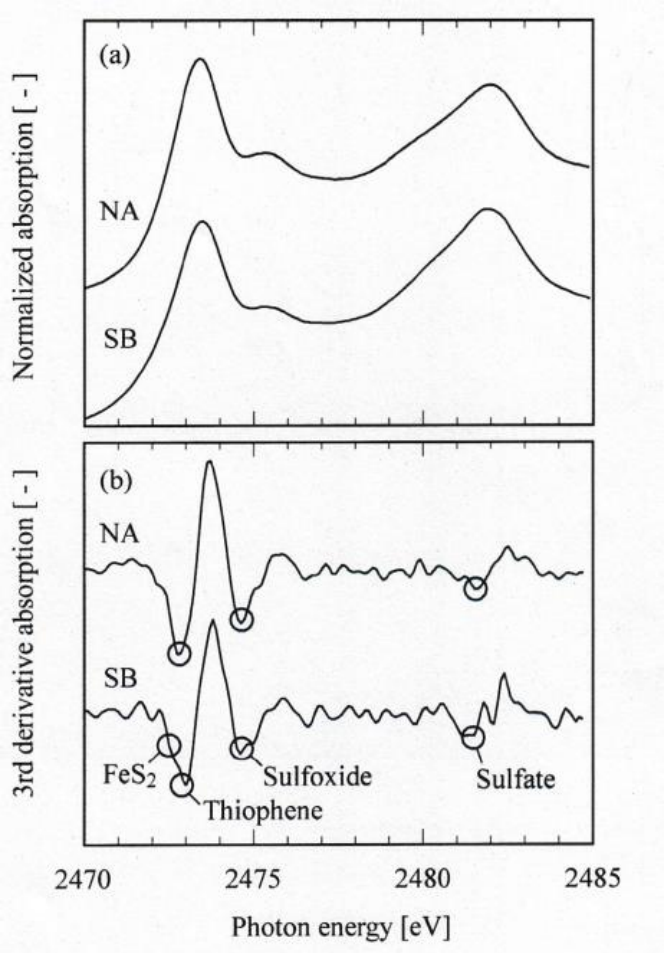

Figure 2.4 (a) Normalized and (b) third-derivative sulfur K-edge XANES spectra of raw SB and NT coals.

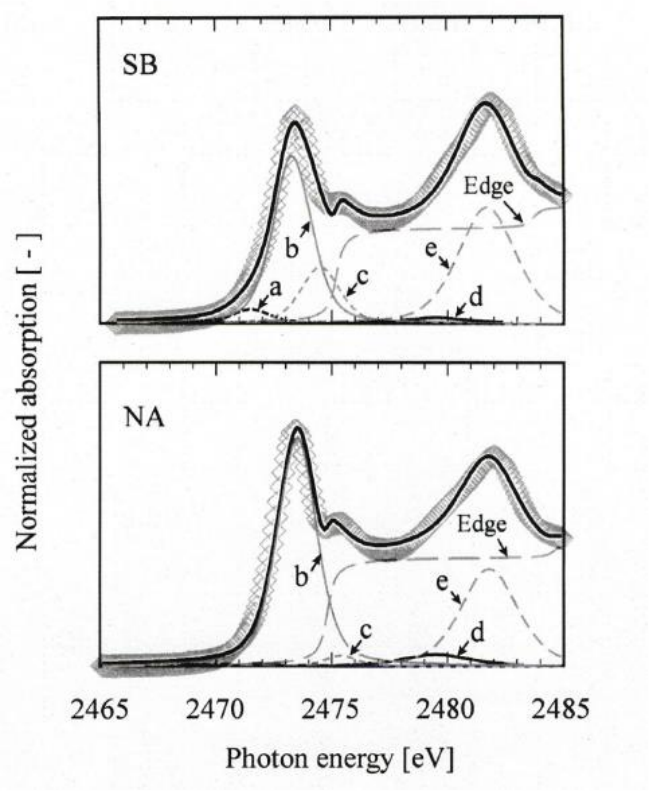

Figure 2.5 Sulfur K-edge XANES spectra of raw SB and NT coals (◇: observed values; thick solid lines: least-squares fits calculated using the peaks of the standard compounds, a: pyrite, b: thiophene, c: sulfoxide, d: sulfone, and e: sulfate).

Table 2.3 Sulfur form distribution in the samples [% of total sulfur]

Sample	Thiophene	Pyrite	Sulfate
	[% of Total sulfur]		
SB	63	28	9
NA	87	6	7

2.3.1 Effect of hydrogen peroxide treatment on subbituminous coal desulfurization

Figure 2.6 shows the sulfur removal extent and the carbon yield with the oxidation time when coal SB is treated with H_2O_2 at 20 and 60 °C. The sulfur removal and carbon yield were determined by the following equations:

$$\text{Sulfur removal rate [\%]} = ((S_0\text{-}S)/S_0) \times 100 \quad (2)$$

$$\text{Carbon yield [\%]} = (C/C_0) \times 100 \quad (3)$$

Where, S_0 and S are the sulfur contents of the raw and oxidized coal respectively, and C_0 and C are the carbon contents of the raw and oxidized coals respectively. All values are on a raw coal basis.

Kato et al., found that the desulfurization of brown coal by H_2O_2 at room temperature, 90% of sulfur removal is achieved within 2h. However, in this study, for coal SB, the desulfurization rate reached only 27% by 2h and there is no significant increase with the increase of the oxidation time. In addition, the change in carbon yield was not significant, suggesting that oxidation H_2O_2 at room temperature hardly changes the organic matrix of SB coal. But, increasing the reaction temperature to 60 °C greatly promoted sulfur removal. Figure 2.7 shows the XANES spectra of SB coal treated at 20 and 60 °C for 24h. The spectrum of oxidized sample at 20 °C was similar to that of raw SB coal showed in Figure 2.4. Figure 2.8 shows the elemental composition of the sample before and after oxidation with H_2O_2 at 20 °C for 24h. Whilst the oxygen content increases after treatment, the decrease in carbon content is as low as 3.85 and the amount of hydrogen remains unchanged, confirming that H_2O_2 is less able to oxidize organic substances and organic sulfur in subbituminous coal at 20 °C.

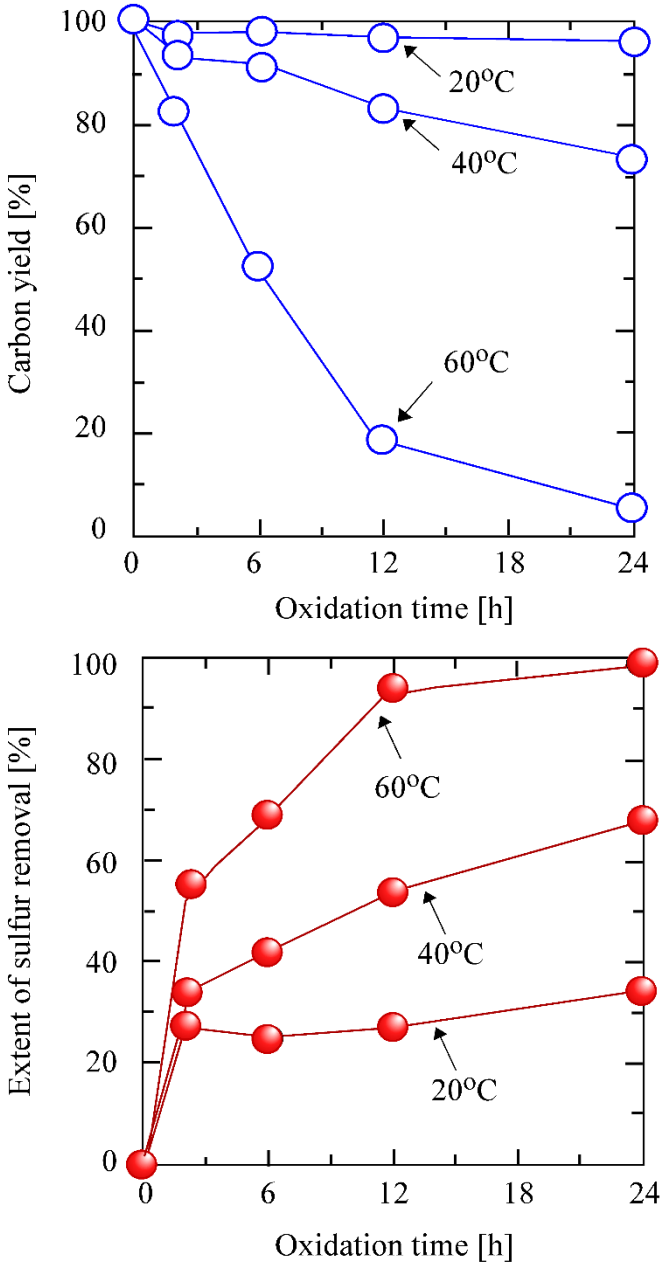

Figure 2.6 Changes in sulfur removal and carbon yield in oxidation of SB coal with H_2O_2 at 20 and 60 °C

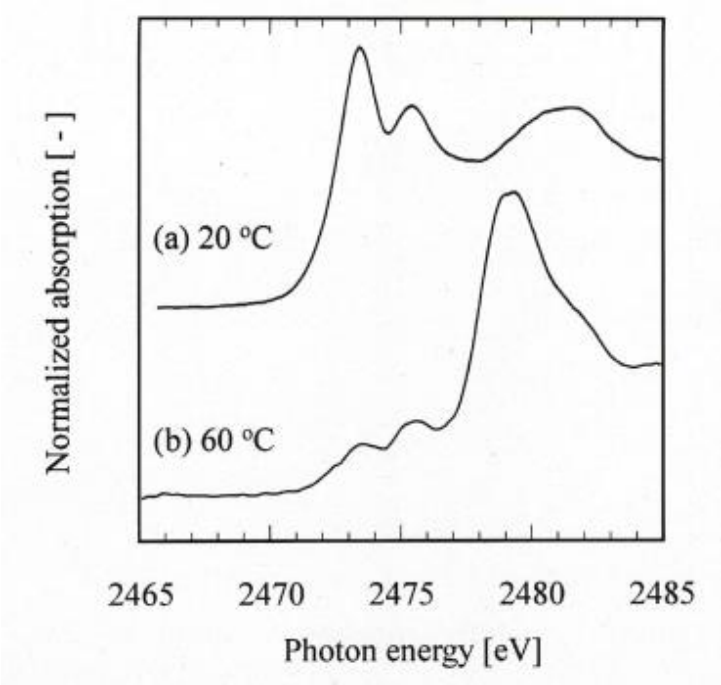

Figure 2.7 Sulfur K-edge XANES spectra of SB coal after oxidation with H_2O_2 at (a) 20 °C and (b) 60 °C for 24h.

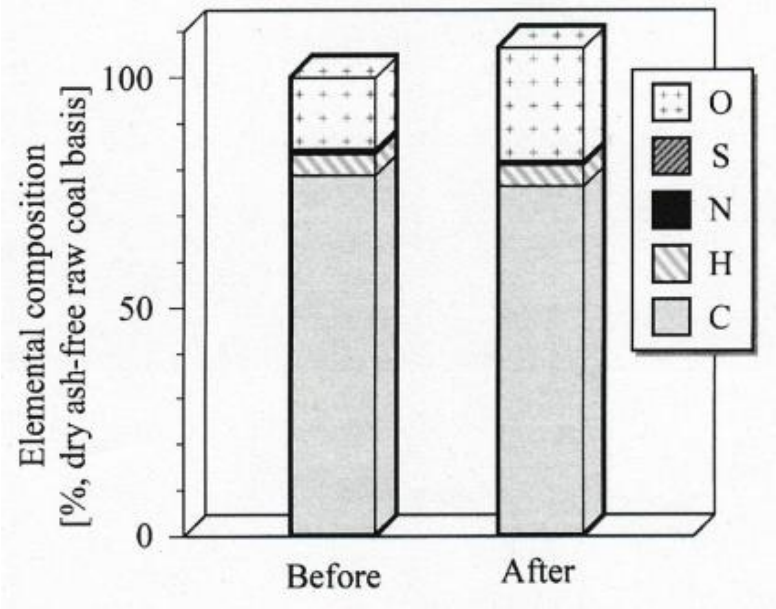

Figure 2.8 Change in elemental composition of SB coal before and after oxidation with H2O2 at 20 °C for 24h.

The abundance ratio of each sulfur form was obtained by least-squares fitting method based on the XANES spectra analysis of SB coal oxidized at 20 °C showed in Figure 2.7.

Figure 2.9 shows the changes in the chemical forms of sulfur (i.e., the pyrite, sulfate, and thiophene ratios) with time. For lignite, the sulfur removed by oxidation was reported to be present as sulfate ions, SO_4^{2-}, in the liquid phase (Kato et al., 2018). Similarly, in this study, it is presumed that the sulfur removed from the solid phase exists in the liquid phase as SO_4^{2-}. It is clear from Figure 2.9 that most sulfur removed at 20 °C is pyrite and inorganic sulfate, while more than 90% of thiophene in the raw coal remained in the solid phase even after 24h. In contrast, when SB coal was treated at 60 °C, the peak at 2473.3 eV decreased and a large peak appeared above 2477 eV, indicating that the sulfur in the treated coal was oxidized; however, this was accompanied by a large loss of carbon showed in Figure 2.6. Thus, although the oxidizing capacity of H_2O_2 increases at higher temperatures, it is not selective toward organic sulfur decomposition. These results indicate that the desulfurization od subbituminous coal using H_2O_2 without significant losses of organic substances is difficult.

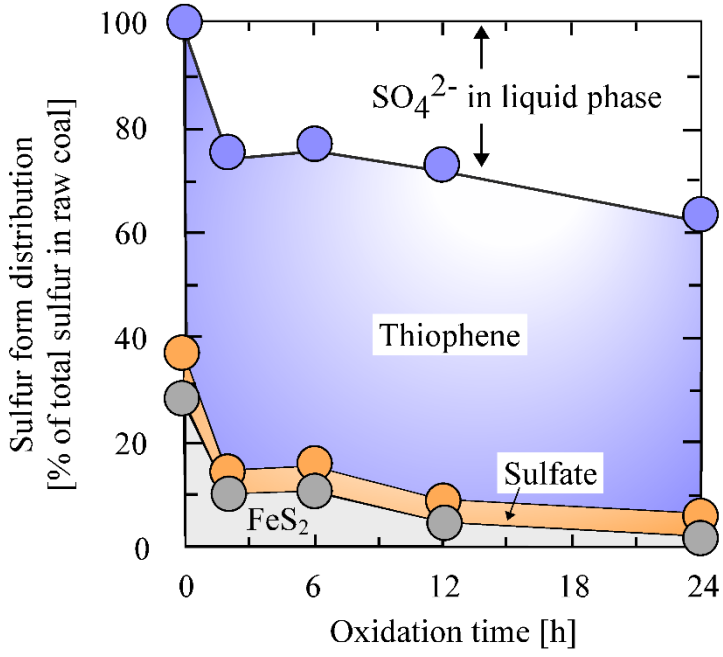

Figure 2.9 Change in sulfur forms after the oxidation of SB coal with H_2O_2 at 20 °C.

2.3.2 Effect of peracetic acid treatment on desulfurization and carbon loss

Figures 2.10 and 2.11 show the effect of reaction time on the sulfur K-edge XANES spectra of SB and NA coals, respectively, after oxidative treatment by peracetic acid (PAA) at 20 °C. In the case of SB coal, the peak of thiophene (2473.3 eV) decreased and that of sulfone (around

2479.5 eV) increased at 6h (Figure 2.10). Additionally, the chemical forms of sulfur did not change from 6 to 24h. Further, it appears that thiophene was more stable in NA coal than in SB coal (Figure 2.11), but oxidation gradually progressed with increasing treatment time.

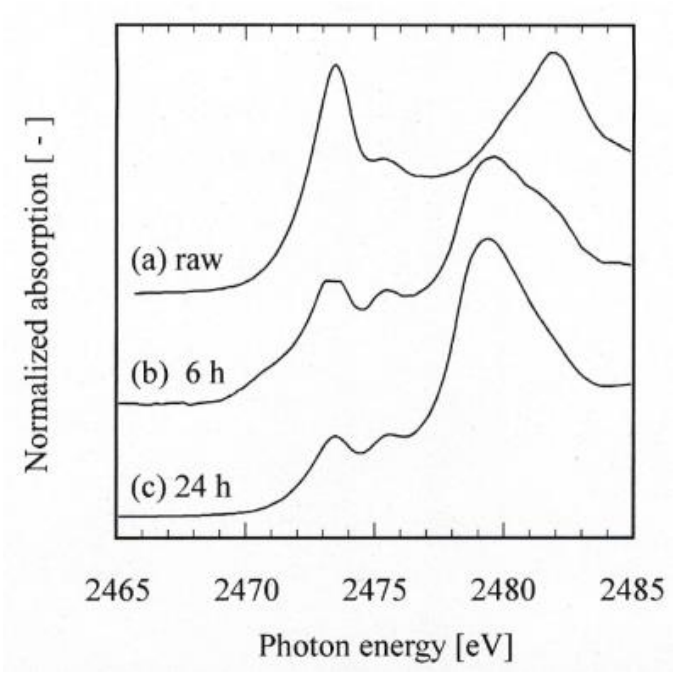

Figure 2.10 Sulfur K-edge XANES spectra of (a) raw SB coal and its oxidized samples treated using PAA at 20 °C for (b) 6 and (c) 24h.

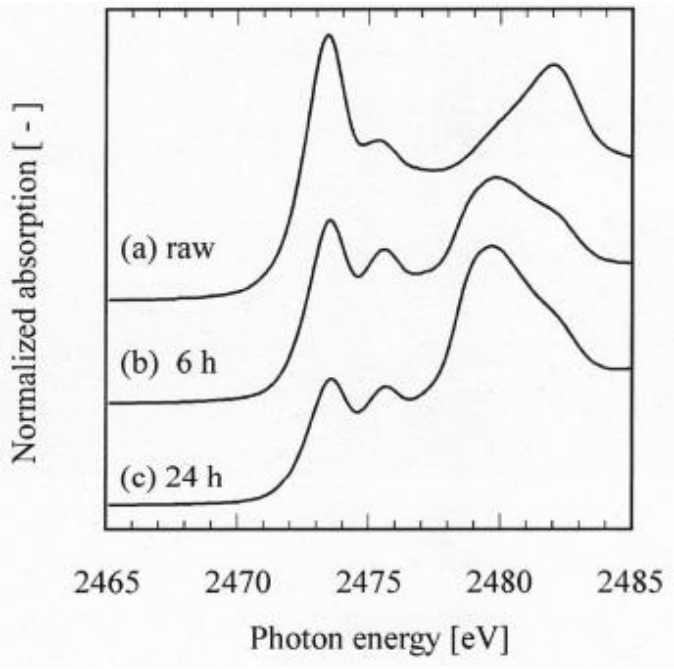

Figure 2.11 Sulfur K-edge XANES spectra of (a) raw NA coal and its oxidized samples treated using PAA at 20 °C for (b) 6 and (c) 24h.

Figures 2.11 and 2.12 shows the effect of time on the carbon yield and sulfur form distribution of SB and NA coals, respectively, after treatment with PAA at 20 °C for 6–24 h. The pyrite in SB coal was completed decomposed within 6h of reaction time. Furthermore, 61% of thiophene in the raw coal was oxidized and converted to sulfone, some of which moved into the liquid phase after 6 h. Additionally, 3% carbon loss was observed at 6h, which did not change significantly upon extending the treatment time. It was confirmed that organic sulfur can be oxidized using PAA without excessively decomposing the organic substances in coal.

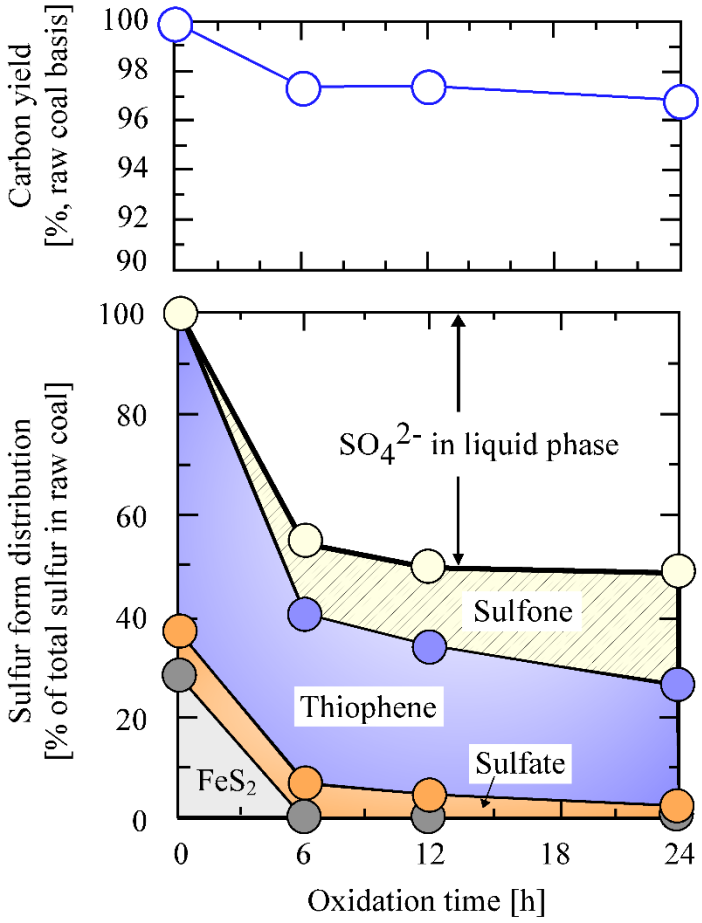

Figure 2.11 Effect of oxidation time on the carbon yield and sulfur form distribution of SB coal treated with PAA at 20 °C.

In the case of NA coal, the decomposition of pyrite was also completed at 6h, but the oxidation rate of thiophene-sulfur was slower than those of SB coal.

There difference in decomposition of thiophene sulfur might be related to the degree of aromaticity of the coals The aromaticity (fa) of NA coal is high (0.83). George G. N. et al., found that carbon content in coals increases linearly with the proportion of thiophene-type

sulfur. So, as the coal rank increases, the amount of stable and less oxidizable thiophene sulfur increases. In this case, NA coal is richer in more stable and aromatic thiophene sulfur than SB coal. Therefore, it is presumed that organic sulfur was chemically stable to the peroxide and that the diffusion resistance of the oxidizing agent into coal particles was high.

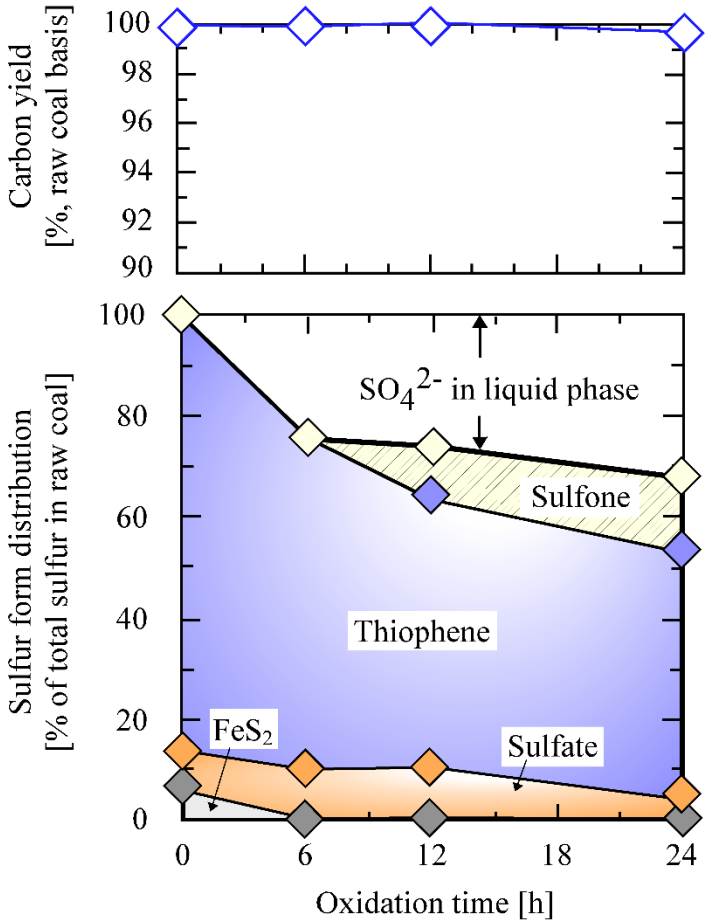

Figure 2.12 Effect of oxidation time on the carbon yield and sulfur form distribution of NA coal treated with PAA.

Assuming that the oxidation by peracetic acid reached equilibrium in 24 h among the thiophenes contained in SB coal and NA coal, the apparent oxidation rate of thiophene in the solid phase, was determined from the following equation:

$$\ln(S_{th}/S_{th,0} = -k(t - t_0) \qquad (4)$$

Where $S_{th,0}$ is the percentage of oxidative thiophene before treatment, and S_{th} is the oxidative thiophene at a predetermined treatment time. In the case of SB coal, k = 3.2×10^{-1} h^{-1}, and in the case of NA coal, k = 1.4×10^{-1} h^{-1}. Figure 2.13 shows the effect of treatment time on the

extent of thiophene conversion in SB and NA coals treated with PAA at 20 °C. It was revealed that the oxidation rate of thiophene in subbituminous coal may differ more than two-fold depending on the type of coal, despite the samples having a similar coal rank.

Figure 2.14 shows the relationship between carbon loss and thiophene conversion for coals treated at 20 °C with H_2O_2 and PAA. The plot in the region above the dashed line, indicates that oxidation of thiophene proceeds in preference to carbon loss. Compared to H_2O_2, PAA does not significantly change the amount of carbon loss, and thiophene sulfur is oxidized. Although the oxidation rate of thiophene sulfur is lower than that of SB coal, thiophene is oxidized in a considerably higher priority than the decomposition of carbon, clearly confirming the effectiveness of PAA for the desulfurization of coal, by conversion of thiophene sulfur. The selectivity of PAA for thiophene sulfur oxidation can be explained by the fact that PAA generated by the reaction of H_2O_2 and acetic anhydride dissociates into acetic acid and hydroxyl cation (OH^+), which is a strong electrophile in acidic solution which reacts with nucleophilic sulfur rather carbon (Borah et al., 2005; De Filippis et al., 2010; Tang et al., 2018), as shown in equation (5).

$$CH_3COOOH + H^+ \rightleftharpoons CH_3COOH + OH^+ \quad (5)$$

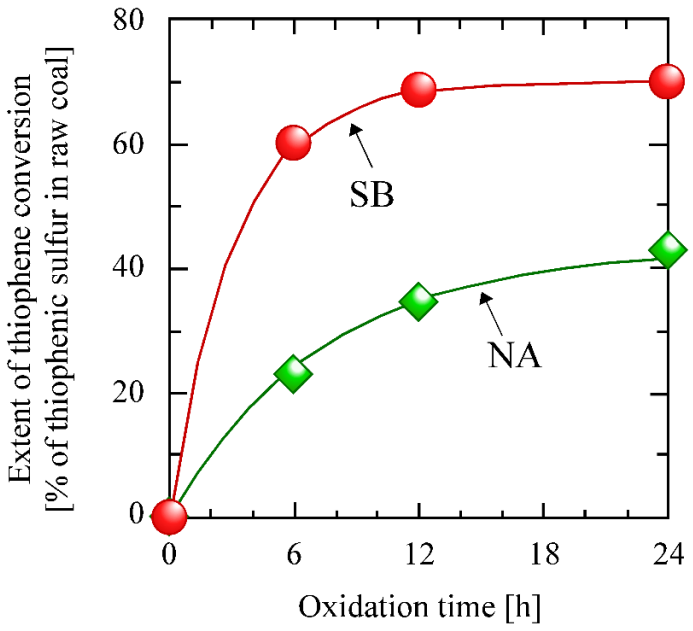

Figure 2.13 Conversion rate of thiophene sulfur in oxidation of SB and NA coals with peracetic acid at 20 °C

Thiophene, which contains a divalent sulfur atom and two lone electron pairs, is rich in electrons and highly nucleophilic and thus selectively reacts with OH^+ (Palmer et al., 1994). The effectiveness of organic peracids for the oxidation of reagent-grade thiophene compounds and thiophene in diesel oil has been reported (De Filippis et al., 2011; De Filippis et al., 2010; Yazu Kazumasa, 2010). In the present study it was concluded that PAA is also effective for desulfurizing subbituminous coal, in particular, for oxidizing thiophene.

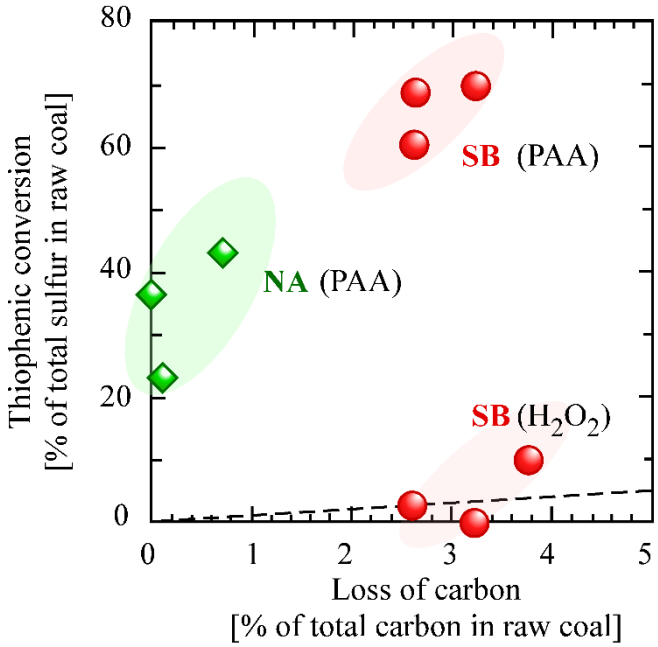

Figure 2.14 Relation between thiophene conversion and loss of carbon in oxidation of coals with H_2O_2 or PAA at 20 °C

2.3.3 Effect of pyrolysis on sulfur removal from oxidized coals

Thiophene was oxidized by treatment with PAA, but a considerable amount of oxidized thiophene remained in the solid phase as sulfone. The removal of thiophene sulfur converted to sulfone was attempted by pyrolysis. The pyrolysis temperature of 400 C was determined as the temperature at which the char yield did not significantly decrease as shown in Figure 2.15. Figure 2.16 shows the carbon yields and sulfur form distribution of oxidized SB and NA coals before and after pyrolysis. After oxidation for 12 h, the oxidized coal was heated up to 400 °C under a nitrogen stream at a heating rate of 5 °C/min. For SB coal, 87% of the original carbon remained in the char after pyrolysis, and the carbon loss due to pyrolysis was less than 6%. The residual sulfur was reduced to 24% and 52% for SB and NA coals, respectively. Despite the samples having a similar coal rank, it was more difficult to remove residual thiophene from oxidized NA coal by pyrolysis than from oxidized SB coal. Nevertheless, it was found in this

study that the pyrolysis characteristics of the produced sulfone-sulfur are similar regardless of the type of coal, and can be removed by thermal treatment at 400 °C without a significant carbon loss.

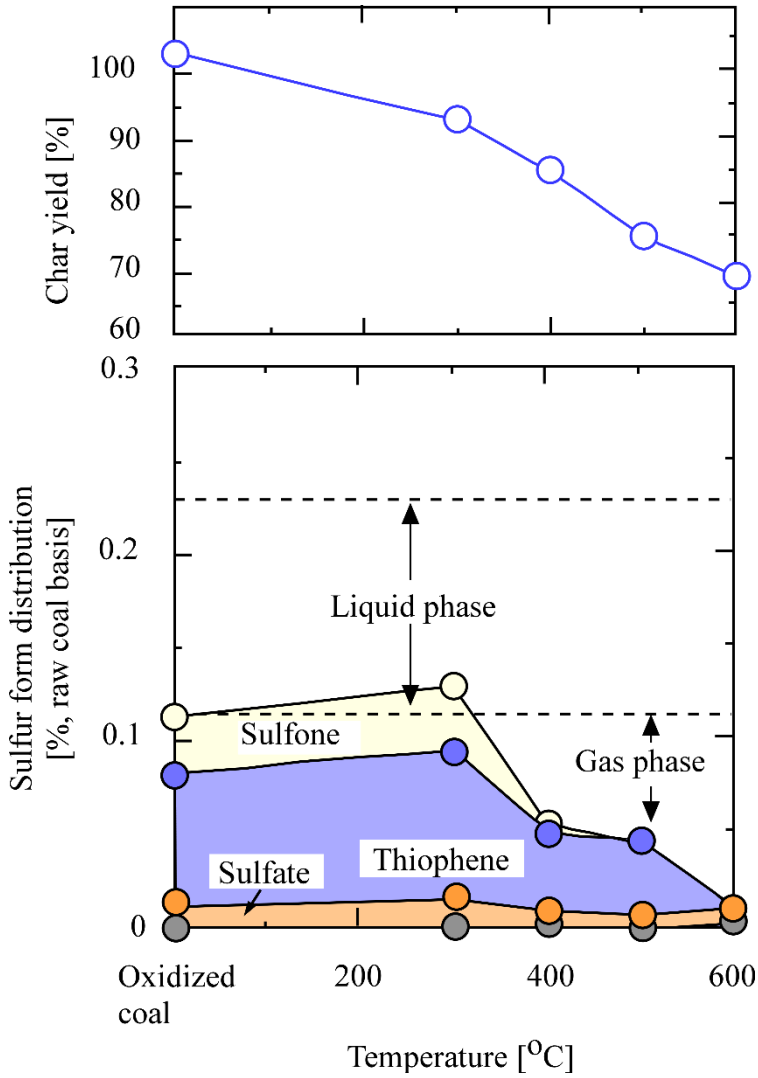

Figure 2.15 Effect of pyrolysis temperature on sulfur form distribution and char yield of PAA oxidized SB coal.

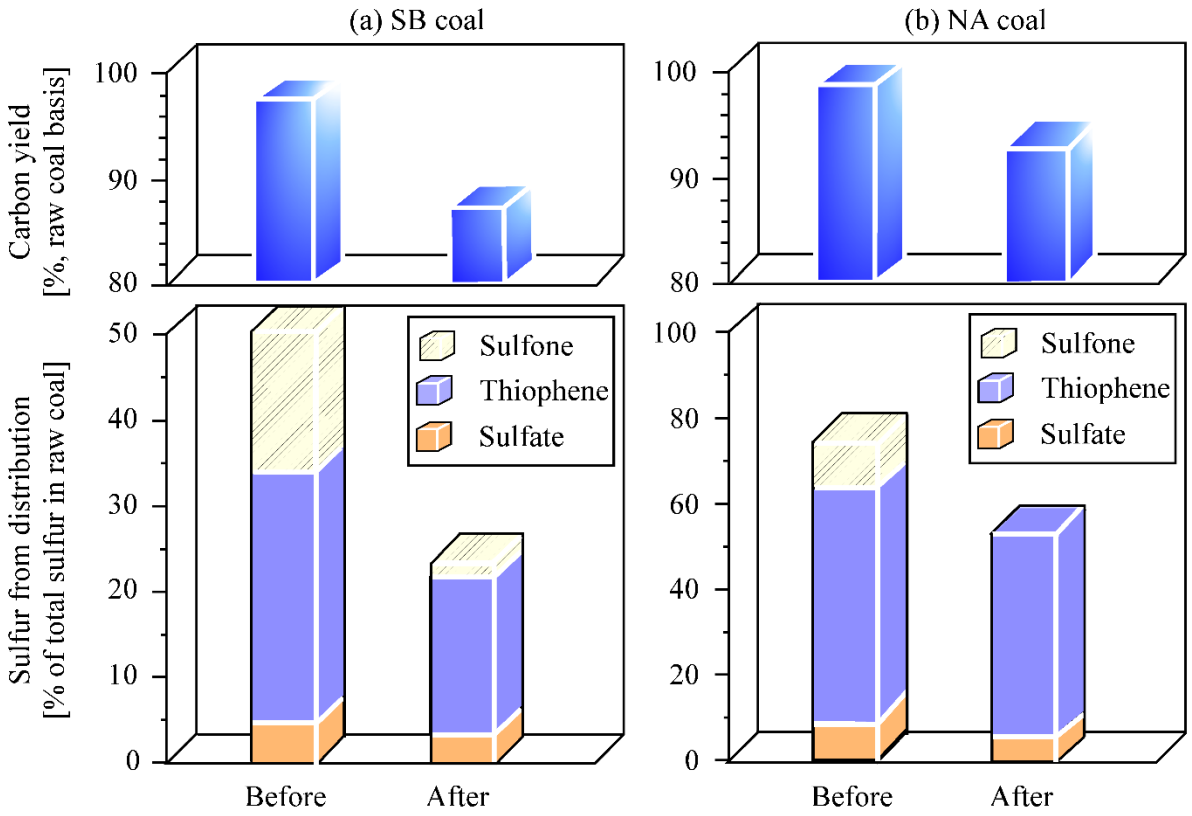

Figure 2.16 Sulfur form distribution and carbon yields before and after pyrolysis of oxidized (a) SB and (b) NA coals (PAA treatment time: 12h; pyrolysis temperature: 400 °C).

2.4 Conclusions

In this study, two kinds of subbituminous coal were oxidized and the effectiveness of oxidative desulfurization was evaluated based on the changes in sulfur content, chemical form of sulfur, and carbon content. Furthermore, the effectiveness of pyrolysis for removing sulfone generated by the oxidation of thiophene was confirmed.

- In treatment by hydrogen peroxide, sulfur removal was promoted, but a large decrease in carbon yield was observed.
- In the other hand, in PAA treatment, selective oxidation of organic sulfur rather than the organic matrix was achieved.
- Thiophene sulfur was oxidized to sulfone form at 20 °C.
- All sulfone generated was removed from both coals without any significant carbon loss after pyrolysis at 400 °C.

Considerations

To improve the conversion and consequent removal of thiophenic sulfur, multi-stage oxidation by peracetic acid could be considered, however, it might result in decomposition of organic matrix and consequently lower carbon yield.

A more efficient alternative for removal of organic sulfur while keeping a high carbon yield is extraction using ionic liquids. Mochizuki and Sugawara (2008), attempted the extraction of thiophene sulfur from a model fuel using halogen-free ionic liquids, and it was demonstrated that a high extraction yield of dibenzothiophene and the extraction yield increased linearly with an increase in the length of alkyl chains and the mass ratio of the ionic liquid to the model fuel.

References

Acharya, C., Kar, R. N., & Sukla, L. B. (2001). Bacterial removal of sulphur from three different coals. *Fuel*, *80*(15), 2207-2216. https://doi.org/10.1016/s0016-2361(01)00100-4

Ali, A., Srivastava, S. K., & Haque, R. (1992). Chemical desulphurization of high sulphur coals. *Fuel*, *71*(7), 835-839. https://doi.org/10.1016/0016-2361(92)90139-f

Aller, Á., MartíNez, O., De Linaje, J. A., Méndez, R., & Morán, A. (2001). Biodesulphurisation of coal by microorganisms isolated from the coal itself. *Fuel Processing Technology*, *69*(1), 45-57. https://doi.org/10.1016/s0378-3820(00)00127-2

Ambedkar, B., Chintala, T. N., Nagarajan, R., & Jayanti, S. (2011). Feasibility of using ultrasound-assisted process for sulfur and ash removal from coal. *Chemical Engineering and Processing: Process Intensification*, *50*(3), 236-246. https://doi.org/10.1016/j.cep.2011.02.008

Borah, D., Baruah, M. K., & Haque, I. (2005). Oxidation of high sulphur coal.9 3. Desulphurisation of organic sulphur by peroxyacetic acid (produced in situ) in presence of metal ions. *Fuel Processing Technology*, *86*(9), 959-976. https://doi.org/https://doi.org/10.1016/j.fuproc.2004.11.015

Çelik, P. A., Aksoy, D. Ö., Koca, S., Koca, H., & Çabuk, A. (2019). The approach of biodesulfurization for clean coal technologies: a review. *International Journal of Environmental Science and Technology*, *16*(4), 2115-2132. https://doi.org/10.1007/s13762-019-02232-7

De Filippis, P., Liuzzo, G., Scarsella, M., & Verdone, N. (2011). Oxidative Desulfurization II: Temperature Dependence of Organosulfur Compounds Oxidation. *Industrial & Engineering Chemistry Research*, *50*(18), 10452-10457. https://doi.org/10.1021/ie200316u

De Filippis, P., Scarsella, M., & Verdone, N. (2010). Oxidative Desulfurization I: Peroxyformic Acid Oxidation of Benzothiophene and Dibenzothiophene. *Industrial & Engineering Chemistry Research*, *49*(10), 4594-4600. https://doi.org/10.1021/ie9017622

Dong, N. S. (2011). Utilisation of low rank coals. *IEA Clean Coal Centre*. https://usea.org/sites/default/files/042011_Utilisation%20of%20low%20rank%20coals_ccc182.pdf

George, G. N., Gorbaty, M. L., Kelemen, S. R., & Sansone, M. (1991). Direct determination and quantification of sulfur forms in coals from the Argonne Premium Sample Program. *Energy & Fuels*, *5*(1), 93-97. https://doi.org/10.1021/ef00025a016

Ghauri, M., Shahzad, K., Inayat, A., Ali, Z., & Cliffe, K. (2016). High Pressure Oxydesulphurisation of Coal Using KMnO4—Effect of Coal Slurry Concentration, pH and Alkali. *Energies*, *9*(4), 289. https://doi.org/10.3390/en9040289

Gonsalvesh, L., Marinov, S. P., Stefanova, M., Carleer, R., & Yperman, J. (2013). Biodesulphurized low rank coal: Maritza east lignite and its “humus-like” byproduct. *Fuel*, *103*, 1039-1050. https://doi.org/10.1016/j.fuel.2012.09.053

Handayani, I., Paisal, Y., Soepriyanto, S., & Chaerun, S. K. (2017). Biodesulfurization of organic sulfur in Tondongkura coal from Indonesia by multi-stage bioprocess treatments. *Hydrometallurgy*, *168*, 84-93. https://doi.org/10.1016/j.hydromet.2016.10.027

Huffman, G. P., Mitra, S., Huggins, F. E., Shah, N., Vaidya, S., & Lu, F. (1991). Quantitative analysis of all major forms of sulfur in coal by x-ray absorption fine structure spectroscopy. *Energy & Fuels*, *5*(4), 574-581. https://doi.org/10.1021/ef00028a008

Kato, T., Nagai, Y., Okawa, H., & Sugawara, K. (2018). Behavior of Sulfur in Liquid Phase Oxidation of Coal. *Journal of the Japan Institute of energy*, *97*(4), 88-96. https://doi.org/10.3775/jie.97.88

Kato, T. N., Yuki; Okawa, Hirokazu; Sugawara, Katsuyasu. (2018). Behavior of Sulfur in Liquid Phase Oxidation of Coal. *Journal of the Japan Institute of energy*, *97*, 88-96.

Kotelnikov, V. I., Saryglar, C. A., & Chysyma, R. B. (2020). Microorganisms in Coal Desulfurization (Review). *Applied Biochemistry and Microbiology*, *56*(5), 521-525. https://doi.org/10.1134/s0003683820050105

Martínez, I., El-Said Mohamed, M., Santos, V. E., García, J. L., García-Ochoa, F., & Díaz, E. (2017). Metabolic and process engineering for biodesulfurization in Gram-negative bacteria. *Journal of Biotechnology*, *262*, 47-55. https://doi.org/10.1016/j.jbiotec.2017.09.004

Mochizuki, Y., & Sugawara, K. (2008). Removal of Organic Sulfur from Hydrocarbon Resources Using Ionic Liquids. *Energy & Fuels*, *22*(5), 3303-3307. https://doi.org/10.1021/ef800400k

Mohebali, G., Ball, A. S., Rasekh, B., & Kaytash, A. (2007). Biodesulfurization potential of a newly isolated bacterium, Gordonia alkanivorans RIPI90A. *Enzyme and Microbial Technology*, *40*(4), 578-584. https://doi.org/https://doi.org/10.1016/j.enzmictec.2006.05.012

Mukherjee, S., & Borthakur, P. C. (2001). Chemical demineralization/desulphurization of high sulphur coal using sodium hydroxide and acid solutions. *Fuel*, *80*(14), 2037-2040. https://doi.org/10.1016/s0016-2361(01)00094-1

Mukherjee, S., & Borthakur, P. C. (2003). Effect of leaching high sulphur subbituminous coal by potassium hydroxide and acid on removal of mineral matter and sulphur☆. *Fuel*, *82*(7), 783-788. https://doi.org/10.1016/s0016-2361(02)00360-5

Mukherjee, S., & Borthakur, P. C. (2004). Demineralization of subbituminous high sulphur coal using mineral acids. *Fuel Processing Technology*, *85*(2-3), 157-164. https://doi.org/10.1016/s0378-3820(03)00140-1

Mukherjee, S., Mahiuddin, S., & Borthakur, P. C. (2001). Demineralization and Desulfurization of Subbituminous Coal with Hydrogen Peroxide. *Energy & Fuels*, *15*(6), 1418-1424. https://doi.org/10.1021/ef010061y

Palmer, S. R., Hippo, E. J., & Dorai, X. A. (1994). Chemical coal cleaning using selective oxidation. *Fuel*, *73*(2), 161-169. https://doi.org/https://doi.org/10.1016/0016-2361(94)90109-0

Ratanakandilok, S., Ngamprasertsith, S., & Prasassarakich, P. (2001). Coal desulfurization with methanol/water and methanol/KOH. *Fuel*, *80*(13), 1937-1942. https://doi.org/10.1016/s0016-2361(01)00047-3

Rossi, G. (2014). The Microbial Desulfurization of Coal. In A. Schippers, F. Glombitza, & W. Sand (Eds.), *Geobiotechnology II: Energy Resources, Subsurface Technologies, Organic Pollutants and Mining Legal Principles* (pp. 147-167). Springer Berlin Heidelberg. https://doi.org/10.1007/10_2013_178

Singh, P. K., Singh, A. L., Kumar, A., & Singh, M. P. (2013). Control of different pyrite forms on desulfurization of coal with bacteria. *Fuel*, *106*, 876-879. https://doi.org/10.1016/j.fuel.2012.11.002

Sönmez, Ö., & Giray, E. S. (2001). The influence of process parameters on desulfurization of two Turkish lignites by selective oxidation. *Fuel Processing Technology*, *70*(3), 159-169. https://doi.org/10.1016/s0378-3820(01)00172-2

Sugawara, K., Tozuka, Y., Sugawara, T., & Nishiyama, Y. (1994). Effect of heating rate and temperature on pyrolysis desulfurization of a bituminous coal. *Fuel Processing Technology*, *37*(1), 73-85. https://doi.org/https://doi.org/10.1016/0378-3820(94)90007-8

Sugawara Katsuyasu, E. Y., Sugawara Takuo, Shirai Masayuki. (2001). XANES analysis of sulfur form change during pyrolysis of coals. *Journal of Synchroton Radiation*, *8*, 955-957.

Tang, L., Fan, H., Guo, J., Zeng, W., & Tao, X. (2018). Investigation on the mechanism of coal desulfurization by ultrasonic with peroxyacetic acid. *Energy Sources, Part A: Recovery, Utilization, and Environmental Effects*, *40*(8), 999-1009. https://doi.org/10.1080/15567036.2018.1468512

Yazu Kazumasa, M. A., Sato Shinya. (2010). Oxidative Desulfurization of Naphtha with Hydrogen Peroxide in Presence of Acid Catalyst in Naphtha/Acetic Acid Biphasic System. *Journal of the Japan Petroleum Institute*, *53*, 251-255. https://www.jstage.jst.go.jp/article/jpi/53/4/53_4_251/_pdf/-char/ja

Chapter 3: Influence of unburned carbon on chemical forms of mercury in fly produced from a coal-fired power plant

3.1 Introduction

Global mercury emissions are projected to increase in the next decades. Streets et al. (2009) suggests that the range of 2050 global mercury emissions are projected to increase to 2390 - 4860 Mg compared to 2480 Mg in 2006. The expansion of coal-fired electricity generation in developing nations is believed to be the main driving force for this increase. In coal combustion, mercury is emitted as Hg^{2+}, Hg^0 and Hg_{-p}. When water soluble Hg^{2+} is deposited to the terrestrial ecosystems and the ocean is reduced to gaseous Hg^0 and it may return back to the atmosphere, prolonging its lifetime in the biosphere (Amos et al., 2014; Amos et al., 2013; Amos et al., 2015; Streets et al., 2018) or it may be involved in methylation-demethylation cycles, resulting in methylmercury (MeHg) which is an especially toxic species (Ariya et al., 2009; López-Antón et al., 2012; Sundseth et al., 2017).

Methylmercury (CH_3HgX) in easily accumulated in fish and shellfish and compared to other forms, it has the highest bioavailability. Many studies found that exposure to CH_3HgX at high concentration can cause a variety of heath complications, including development impairment, reduced reproductive success, induced liver and kidney damage and immunomodulation (Chen & Wilcox, 2008; Leonard I. Sweet, 2001; Scheuhammer & Sandheinrich, 2008; Yang et al., 2020).

The Minamata disease is an example of a large scale poisoning by CH_3HgX which resulted in increasing cases of behavioral, neurochemical, hormonal and immunological disorders (Eto, 1997; Semionov, 2018).

In coal fired-power plants, the emissions of mercury are reduced by air pollution control devices, by being captured and recovered together with fly ash and desulfurization gypsum. However, more stable Hg0 that is not captured in this process, is released into the atmosphere. With the growing efforts and regulations of mercury emissions (Scientific, 2019), to advance the capability of fly ash and desulfurization gypsum to capture mercury, it is important to clarify the mercury forms in these byproducts and their release patterns.

Methods of identifying mercury chemical forms contained in coal combustion byproducts include sequential chemical extraction (Han et al., 2003; Kim et al., 2003; Zhu et al., 2016), temperature-programmed desorption (Liu et al., 2013), X-ray absorption fine structure (XAFS) (Huggins et al., 2003; Kim et al., 2003; Kim et al., 2004), X-ray absorption near edge structure (XANES) (Esbrí

et al., 2010; Liu et al., 2016) and the recently developed method that combines temperature-programmed desorption and cold vapor atomic absorption (TPD-CVAAS) (Sakusabe et al., 2019, 2020).

In this study, XANES analysis was used for the determination and speciation of mercury in the fly ash. The effects of sulfur contained in the unburned carbon were investigated.

3.2 Experimental

3.2.1 Sample

A fly ash collected from an actual coal-fired power plant was sieved to obtain a rich fraction of unburned carbon. The sample contained 2.6 ppm of mercury and 27.1 wt% of carbon content. Additionally, the fly ash sample was sieved to four level of 42,53,72, and 96 μm average size.

3.2.2 Mercury model samples

Six types of mercury compounds, namely: Hg (GR, Wako Pure Chemical Industries), Hg_2Cl_2 (GR, Wako Pure Chemicals), $HgCl_2$ (GR, Wako Pure Chemicals), HgS (cinnabar, GR, Kanto Chemicals), $HgSO_4$ (GR, Wako Pure Chemicals), HgO (GR, Nacalai Tesque) were also used without purification. And a range of organic mercury samples such as sodium ethyl mercury thiosalicylate, phenylmercuric acetate (GR, Nacalai Tesque), and ethyl mercury chloride (Environmental Research grade: ER, Kanto Chemicals) These organic mercury samples were selected to estimate the binding forms of mercury adsorbed on unburnt carbon, which, as indicated by their structures, are -C-Hg-S, -C-Hg-O and -C-Hg-Cl- respectively.

3.2.3 Preparation of mercury-adsorbed unburned carbon

Unburned carbon sample was extracted from fly ash by successively boiling the fly ash in 46% hydrofluoric acid (HF) and 6M of hydrochloric acid (HCl) at 110 °C for 1h. This procedure was repeated 3 times until a rich fraction of unburned carbon was obtained. The obtained unburned carbon was then heated at 700 °C to remove mercury. The mercury-free unburned carbon was exposed to HgO vapor at 900 °C to prepare mercury-adsorbed unburned carbon (UC-Hg).

3.2.4 Preparation of sulfur-impregnated mercury-adsorbed unburned carbon

To study the effect of sulfur on mercury forms on unburned carbon, a sample abbreviated as UCS-Hg was prepared from the unburned carbon sample. Unburned carbon was mixed with elemental sulfur at 1:1 mixing ratio and heated to 600 °C, under nitrogen stream. The sulfur-impregnated unburned carbon was then exposed to HgO vapor at 900 °C to obtain the sulfur-impregnated mercury-adsorbed unburned carbon.

3.3 Analyses

3.3.1 Quantification of carbon and sulfur

Carbon content in fly ash was measured by NCH analyzer (Sumika Chemical Analysis Service, NCH-22) and the sulfur content was measured by a carbon sulfur analyzer (Horiba, EMIA 220V).

3.3.2 Fly ash surface morphology

The average particle size distribution of the fly ash was measured using a laser diffraction (Microtrac MT 3000 II, Nikkiso Corp.). And the surface of was observed using a scanning electron microscope (SEM-EDX, JSM-7800F, JEOL Corp.).

3.3.3 Measurement of total mercury content

The mercury content in the fly ash was measured by TPD-CVAAS method developed by Sakusabe et al. (2019). Here, the mercury compound in fly ash is heated to 700 °C under argon gas stream and desorbed from the sample in an electric tubular furnace, and the generated mercury compound vapor is bubbled into a 90 g / mℓ stannic chloride solution where is reduced to elemental mercury. After that, it passed through an absorption tube of calcium chloride, and atomic absorption was measured with an atomic absorption spectrophotometer installed on the downstream side.

3.3.4 Identification and quantification of mercury forms

The analysis of mercury forms on fly ash and unburned carbon samples was performed by measuring the XANES spectrum of Hg LIII-edge using beam lines (BL) 9A and 12C of the Photon Factory at High Energy Accelerator Research Organization in Tsukuba, Japan. As described by Uaciquete et al. (2021), the samples were mixed with boron nitride and pressed at 2 ton.com-2 using a tablet molder. Under atmospheric pressure conditions, X-rays varied in energy by rotation

of a Si (111) double crystal monochromator were used to irradiate the samples, and the X-ray fluorescence generated from the samples was monitored by a multi-element germanium detector. The range of X-ray energy irradiated to the samples was from 12,236 eV to 12,588 eV. The irradiated energy was calibrated using the 12,284 eV peak of the elemental mercury XANES spectrum (Uaciquete et al., 2021).

The estimation of chemical forms was estimated by the inflection point method proposed by Huggins et al. (2003). In this method, the inflection point difference (IPD) defined from the first derivative spectra and is calculated by the following equation:

$$\text{Inflection point difference } (\Delta E) = E_2 - E_1 \qquad (6)$$

Where, E_1 and E_2 represent the minimum and maximum adsorption threshold which is defined as the energy at which the open continuum channel for photo-electric absorption becomes available, producing continuum photo electron. Or simply the positions of lower energy and higher energy peaks in the first derivative spectra respectively (Huggins et al., 2003).

And the chemical forms of the samples were estimated by comparing the IPD values of the samples to those of the model compounds.

The quantitative analysis was performed by linear combination fitting of the obtained XANES spectra with the XANES spectra of the model mercury compounds, and the abundance ratio of each form was determined from the proportion of each linearly combined spectrum.

Normalization, smoothing and differential of XANES spectra were carried out using the software, Athena (IFEFFIT) and Excel (Microsoft Office) (Uaciquete et al., 2021).

3.4 Results and Discussion

3.4.1 Effect of carbon on mercury

The SEM image of unburned (Figure 3.1) carbon show glassy surface containing many pores of <1 μm. And in the EDX analysis, sulfur, chlorine and oxygen were detected.

Figure 3.2 shows the correlation between the mercury and carbon contents measured in the sieved fly ash. Although no correlation was found between the mercury content and the average size of the fly ash, a linear correlation was found between the mercury content and the carbon content in the different sieving levels (42, 53, 72 and 96 μm) of fly ash.

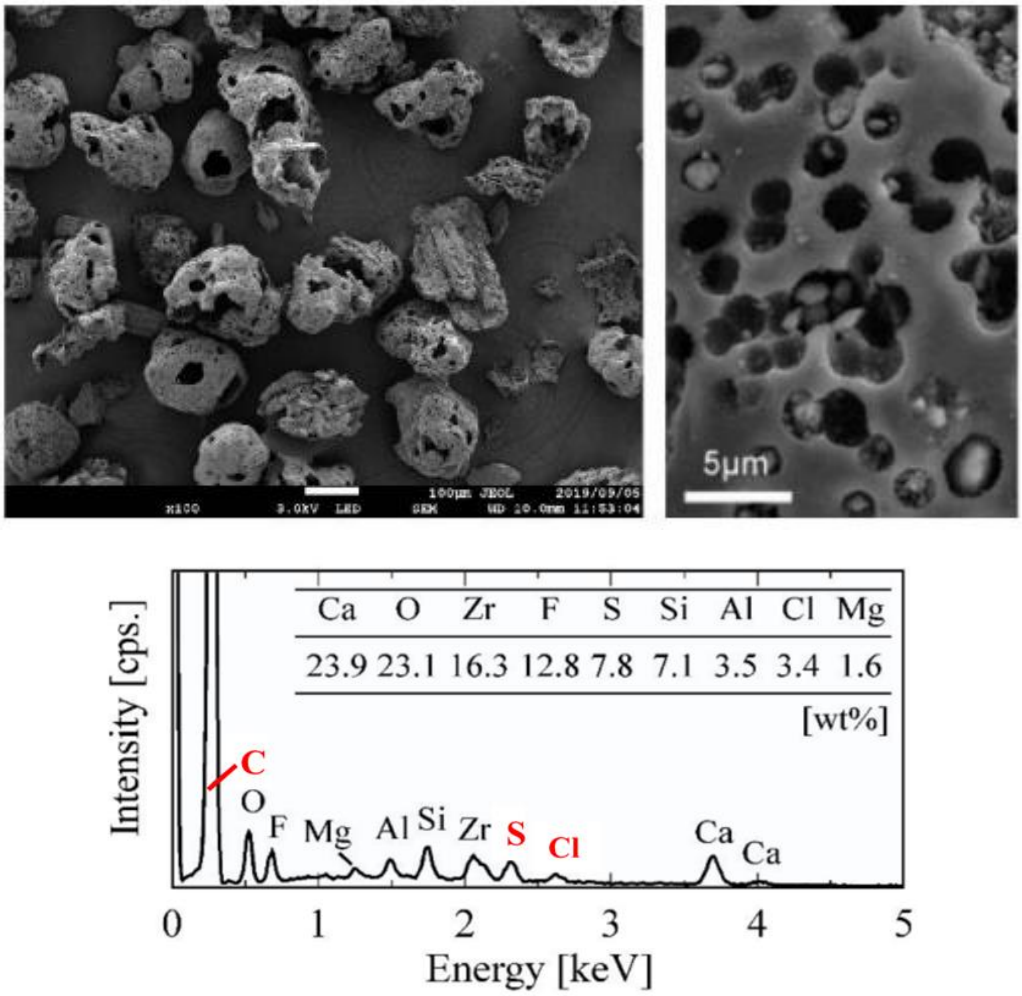

Figure 3.1 SEM and EDX analyses of unburned carbon

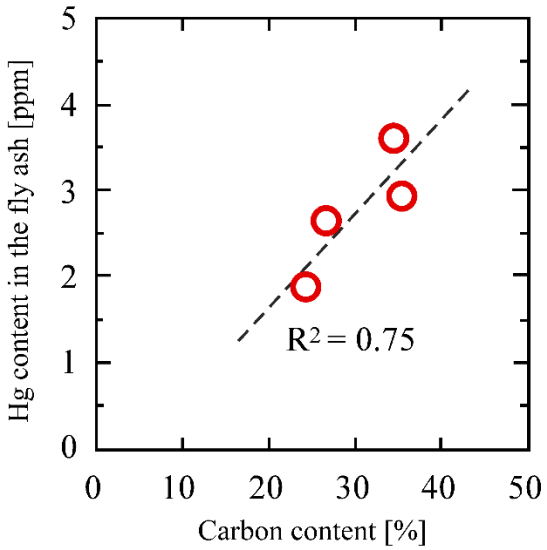

Figure 3.2 Relationship between mercury and carbon contents in fly ash

3.4.2 XANES spectra of mercury model samples

The obtained XANES spectra of the model sample mercury compounds are shown in Figure 3.3. And the Figure 3.4 shows the first derivative of the obtained XANES spectrum. he energies E_1 and E_2 with the maximum slope of the absorption edge were determined from Figure 3.4, and the difference ΔE values were calculated.

The ΔE values are listed from the highest to the lowest. Huggins et al.,(1999; 2003) found that the positions and the relative intensities of E_1 and E_2 peaks reflect the chemical bonding of the nearest neighbour (NN) coordination sphere around the mercury ion. inflection point difference (IPD) correlates the differences in the ionicity of the Hg – NN bond. The more ionic compounds of mercury, such as HgO, in which the Hg ion is surrounded by relatively small, ionic oxygen anions, have large IPD values, whereas the least ionic and largest anionic species, such as S^- in Hg sulfides, give smaller IPD values. This is in accordance with the ΔE values for each mercury compound model sample shown in Table 3.1. The ΔE of elemental mercury could not be calculated because an obvious peak at E_2 was not observed.

As an example of the first and second derivative of XANES spectra of $HgSO_4$, Figure 3.5 shows that XANES spectrum of $HgSO_4$.

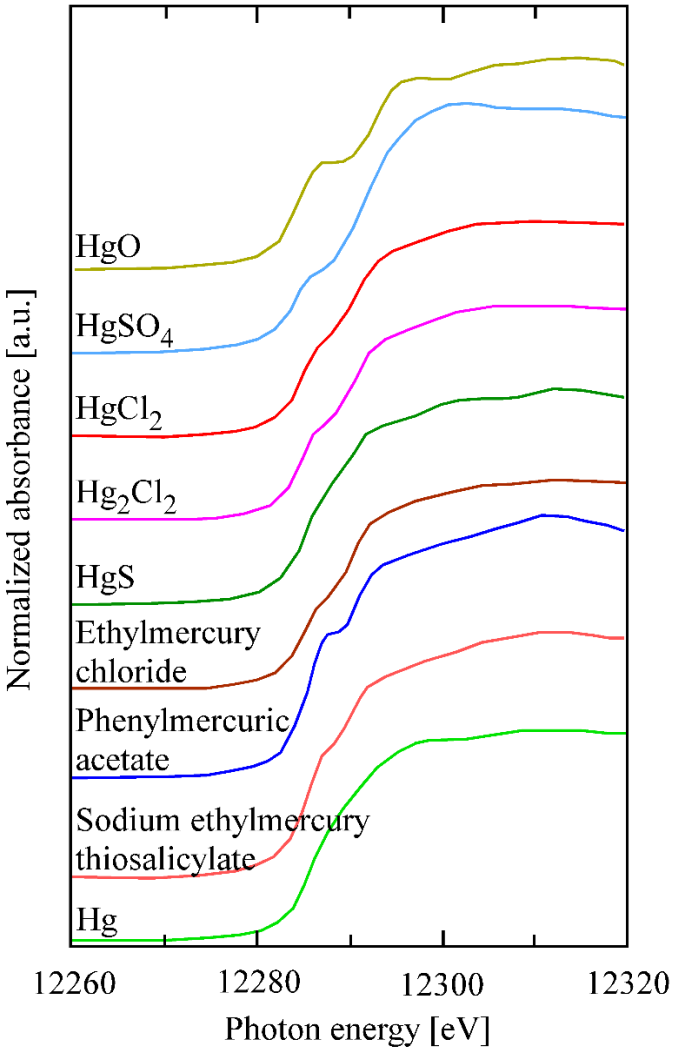

Figure 3.3 Hg L_{III} edge XANES spectra of model Hg compounds

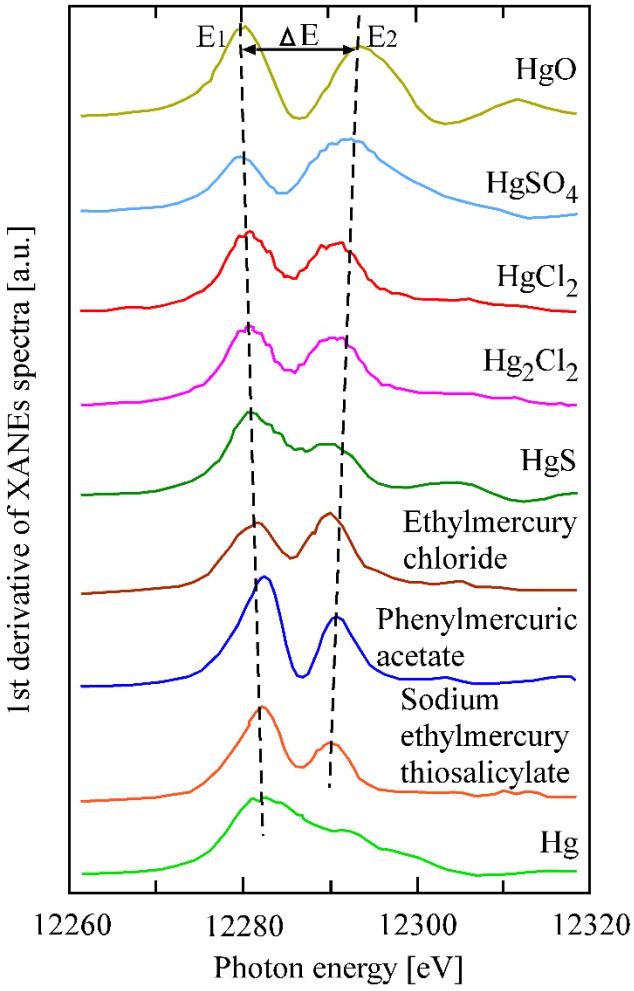

Figure 3.4 First order derivative of XANES spectra of model Hg compounds

Table 3.1 Inflection point difference from Hg XANES spectra of model compounds

Mercury compound	Inflection point difference ΔE (eV)
HgO	13.5
$HgSO_4$	12.3
Hg_2Cl_2	10.3
$HgCl_2$	10.3
HgS	8.9
Ethylmercury Chloride	8.4
Phenylmercuric acetate	8.4
Sodium ethylmercury thiosalicylate	7.9

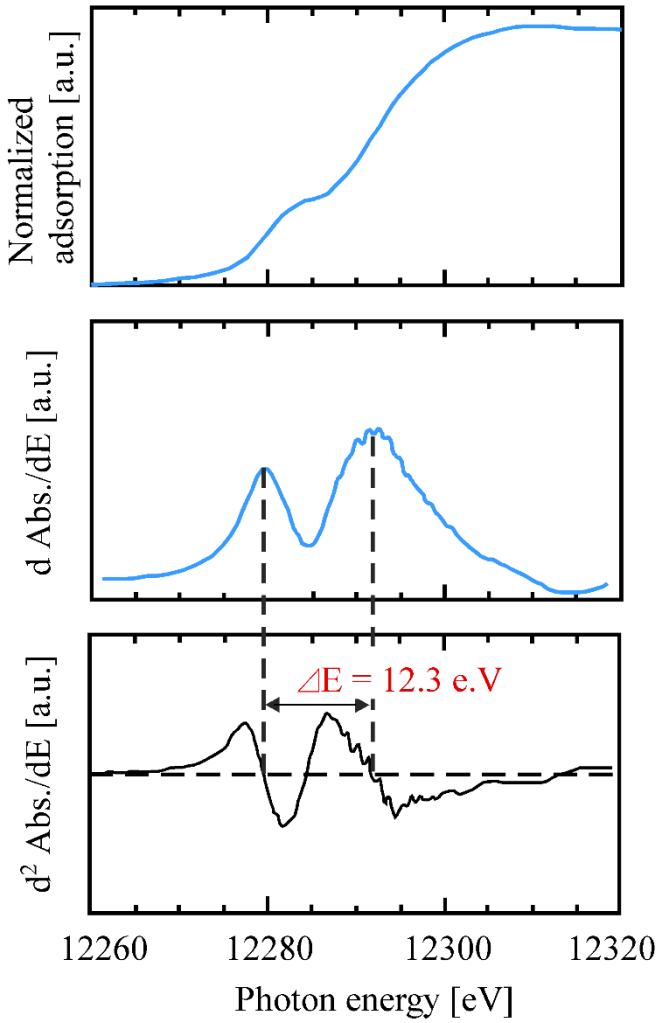

Figure 3.5 Inflection point difference from XANES spectrum of $HgSO_4$ model sample

3.4.3 XANES spectrum of fly ash containing unburned carbon

Figure 3.6 shows the Hg XANES spectrum and its first derivative curve for the fly ash samples containing the unburned carbon. ΔE was measured as 7.9 eV, which more closely resembles to control value of organic mercury rather than the inorganic mercury compounds; however, this value does not precisely match with any of the observed ΔE of the model compounds.

In addition, the XANES spectra of the HgO and HgS, and their mixture at 1:1 weight ratio, were anayzed. The XANES spectrum of the mixture of HgO and HgS was modeled by linear combination fitting of the XANES spectra of HgO and HgS. The observed XANES spectrum of the mixture, the modeled values as well as the residual values between the observed and modeled values are shown in Figure 3.7. As it is shown, the XANES spectrum of the mixture of HgO and HgS can be accurately modeled using the XANES spectra of HgO and HgS with their abundance ratio as a fitting parameter.

The linear combination fitting using XANES spectra of modeled compounds was thus used to estimate the chemical forms of mercury and their relative abundance ratio in the fly ash sample, and the modeled results can be seen in Figure 3.8. The XANES spectrum of the fly ash was modeled successfully using the spectra of model compounds and Table 3.2 shows the estimated abundance ratio of the mercury chemical forms contained in the fly ash. Mercury in the fly ash appears to be bound with S, Cl and O compounds. This behavior can be explained by the fact that in flue gas of coal-fired power plants, H_2S and SO_2 may react with unburned carbon and generate sulfuric functional groups (Sugawara et al., 2003), which then react with gaseous mercury and produce the types of mercury bound to sulfur and oxygen found in the unburned carbon.

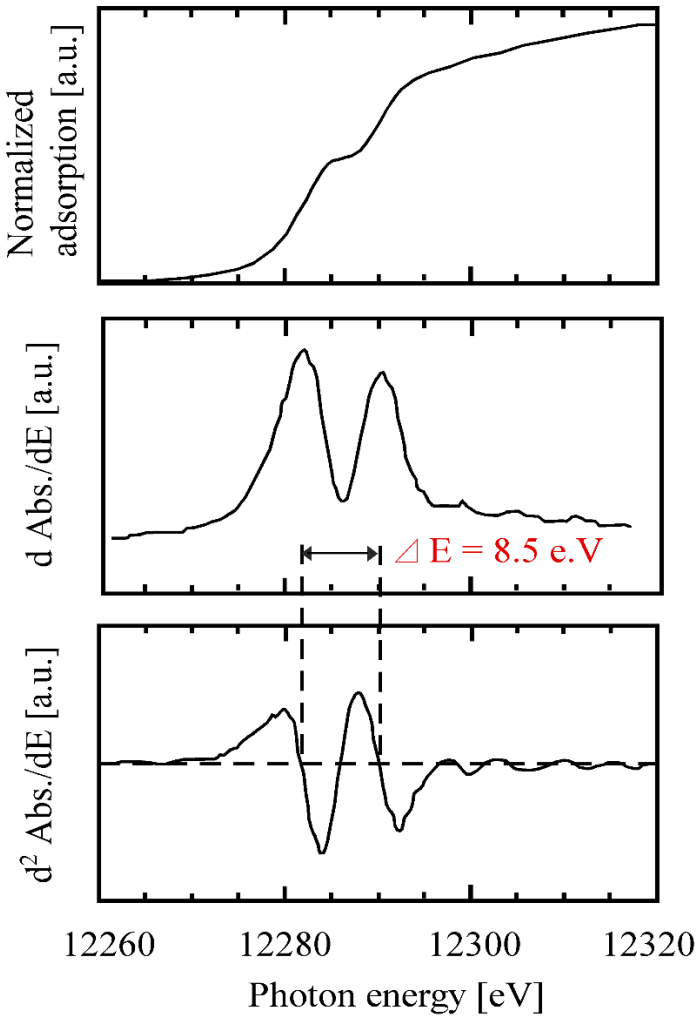

Figure 3.6 XANES spectra, first and second derivatives of the fly ash.

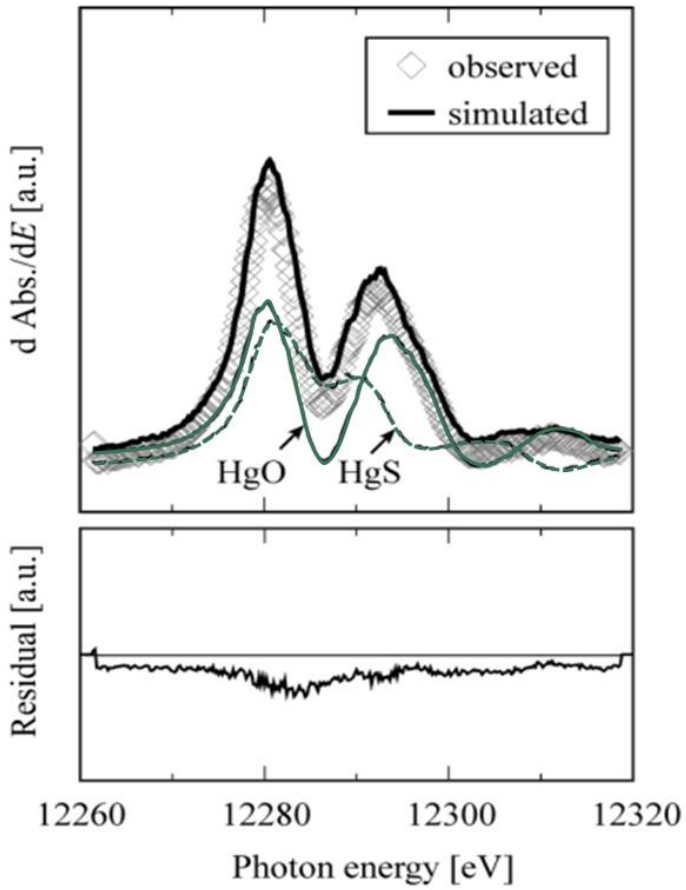

Figure 3.7 XANES spectra of HgO and HgS mixture.

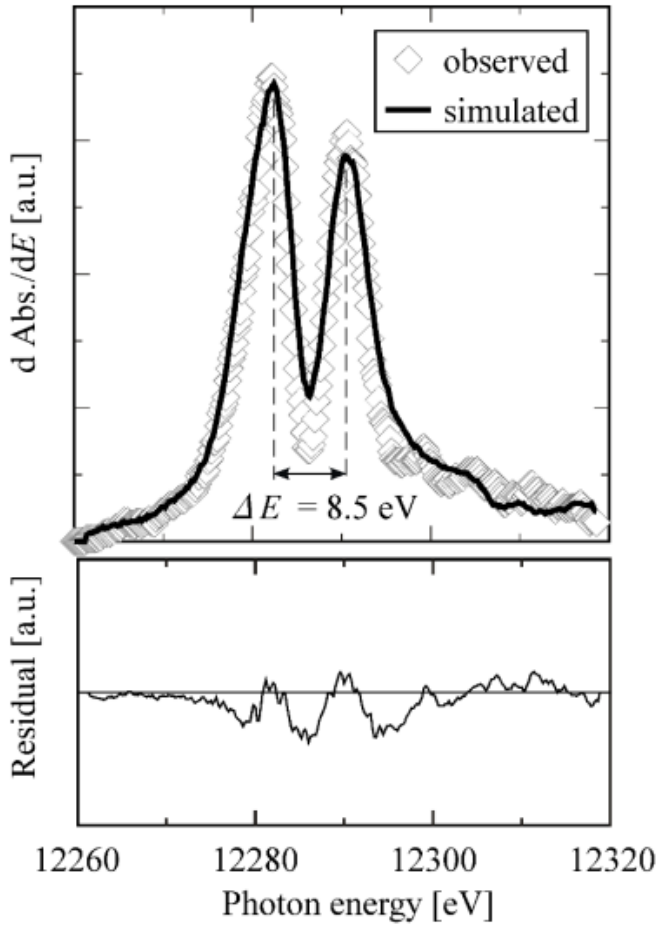

Figure 3.8 First derivative of XANES spectra for the fly ash and simulated curve by using XANES spectra of model compounds.

Table 3.2 Total mercury content and estimated abundance ratio of mercury forms in the fly ash

Hg [ppm]	Abundance ratio [%]			
	$HgSO_4$	C(C)S[Hg]	C [Hg]Cl	C[Hg]O
2.6	18	18	27	36

3.4.4 XANES spectra of modeled unburned carbon

The XANES spectrum of UC-Hg was measured to clarify the chemical forms of mercury when captured by unburned carbon in the gaseous phase. Figure 3.9 shows the first and second derivatives of the UC-Hg. The calculated IPD value was 8.3 eV which is close to those of the organic mercury compounds, ethyl mercury chloride (8.4 eV), phenylmercuric acetate (8.4 eV) and sodium ethylmercurithiosalicylate (7.9 eV).

The XANES spectrum of the UCS-Hg is represented in Figure 3.10. Similarly, to UC-Hg the IPD value of UCS-Hg is close to those of the organic compounds, indicating the formation of compounds of organic sulfur with mercury.

Since the IPD value of these samples was similar to those of the mercury organic compounds (ethyl mercury chloride, phenylmercuric acetate and sodium ethylmercurithiosalicylate), the spectra of UC-Hg and UCS-Hg were simulated using these compounds. Figure 3.11 shows the derivative spectra and their respective simulated curves. The total captured mercury captured increased from 33 ppm in UC-Hg to 155ppm in UCS-Hg as the sulfur content increased from 0.08% in UC to 3.4% in UCS.

The sulfur content in the unburned carbon considerably increases the quantity and forms of mercury captures by unburned carbon as shown in Table 3.3. This might indicated that there is a possibility that unburned carbon reacts with gaseous sulfuric compounds such as SO_2 and H_2S in the flue gas when moving from the boiler to the electrostatic precipitator (Uaciquete et al., 2021). In this study it was demonstrated that gaseous mercury is more easily captured by sulfur, chlorine as well as oxygen compounds in the fly ash containing the unburned carbon.

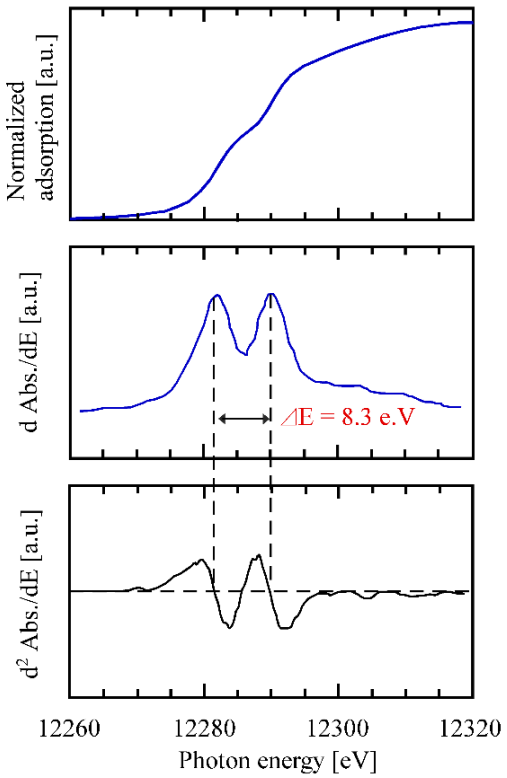

Figure 3.9 XANES spectra, first and second derivatives of UC-Hg

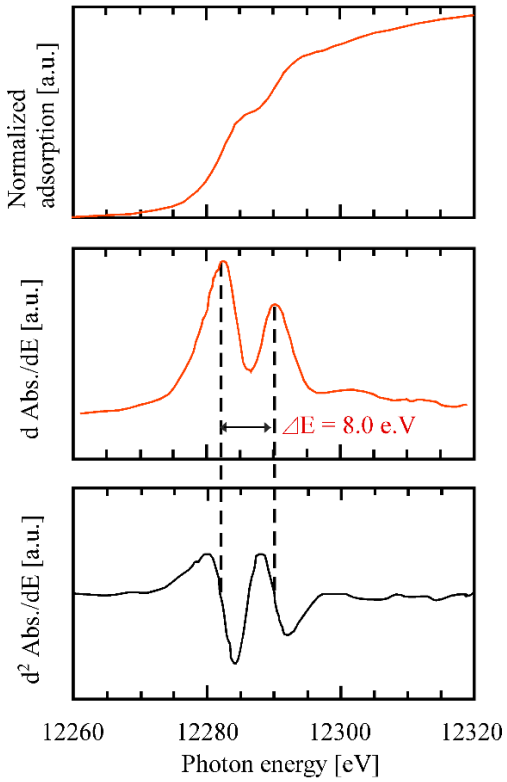

Figure 3.10 XANES spectra, first and second derivatives of UCS-Hg

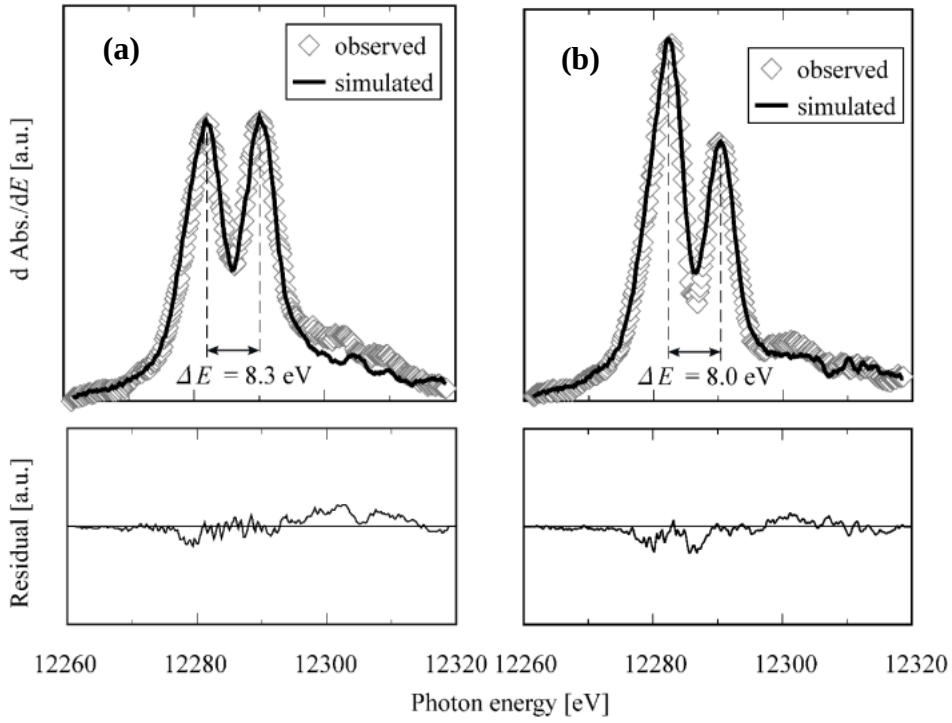

Figure 3.11 First derivatives of XANES spectrum for (a) UC-Hg and (b) UCS-Hg and simulated curves by using XANES spectra of model compounds

Table 3.3 Total content of Hg and estimated abundance ratio of Hg forms of UC-Hg and UCS-Hg

Sample	Hg [ppm]	Abundance ratio [%]		
		C(C)S[Hg]	C [Hg]Cl	C[Hg]O
UC-Hg	3.3	16	80	4
UCS-Hg	155	64	21	15

3.5 Conclusions

Mercury chemical forms in fly ash containing unburned carbon were determined by XANES analysis. The total content of mercury was proportional to the carbon content of the fly ash. XANES spectra of the fly ash were modeled by linear combination fitting using XANES spectra of control mercury compounds.

In order to clarify the effect of unburned carbon on mercury's chemical forms, two types of model mercury-adsorbed unburned carbon with and without sulfur impregnation.

- Total content of mercury was proportional to the carbon content of fly ash.
- The mercury forms in the fly ash were found to be sulfur, chlorine or oxygen compounds.
- All mercury in the UC-Hg and UCS-Hg was bound to sulfur, chlorine and oxygen compounds.
- Mercury content increased drastically with the increase of the sulfur content.
- Amount of mercury is dependent on the unburned carbon content.
- Mercury chemical forms is strongly influenced by the presence of sulfur, chlorine and oxygen in the unburned carbon.

References

Amos, H. M., Jacob, D. J., Kocman, D., Horowitz, H. M., Zhang, Y., Dutkiewicz, S., Horvat, M., Corbitt, E. S., Krabbenhoft, D. P., & Sunderland, E. M. (2014). Global biogeochemical implications of mercury discharges from rivers and sediment burial. *Environ Sci Technol*, *48*(16), 9514-9522. https://doi.org/10.1021/es502134t

Amos, H. M., Jacob, D. J., Streets, D. G., & Sunderland, E. M. (2013). Legacy impacts of all-time anthropogenic emissions on the global mercury cycle. *Global Biogeochemical Cycles*, *27*(2), 410-421. https://doi.org/10.1002/gbc.20040

Amos, H. M., Sonke, J. E., Obrist, D., Robins, N., Hagan, N., Horowitz, H. M., Mason, R. P., Witt, M., Hedgecock, I. M., Corbitt, E. S., & Sunderland, E. M. (2015). Observational and Modeling Constraints on Global Anthropogenic Enrichment of Mercury. *Environmental Science & Technology*, *49*(7), 4036-4047. https://doi.org/10.1021/es5058665

Ariya, P. A., Peterson, K., Snider, G., & Amyot, M. (2009). Mercury chemical transformations in the gas, aqueous and heterogeneous phases: state-of-the-art science and uncertainties. In R. Mason & N. Pirrone (Eds.), *Mercury Fate and Transport in the Global Atmosphere: Emissions, Measurements and Models* (pp. 459-501). Springer US. https://doi.org/10.1007/978-0-387-93958-2_15

Chen, C., & Wilcox, B. A. (2008). Ecotoxicology of Methylmercury: A Transdisciplinary Challenge. *EcoHealth*, *5*(4), 393-395. https://doi.org/10.1007/s10393-009-0214-4

Esbrí, J. M., Bernaus, A., Ávila, M., Kocman, D., García-Noguero, E. M., Guerrero, B., Gaona, X., Álvarez, R., Perez-Gonzalez, G., Valiente, M., Higueras, P., Horvat, M., & Loredo, J. (2010). XANES speciation of mercury in three mining districts – Almadén, Asturias (Spain), Idria (Slovenia). *Journal of Synchrotron Radiation*, *17*(2), 179-186. https://doi.org/10.1107/s0909049510001925

Eto, K. (1997). Review Article: Pathology of Minamata Disease. *Toxicologic Pathology*, *25*(6), 614-623. https://doi.org/10.1177/019262339702500612

Han, Y., Kingston, H. M., Boylan, H. M., Rahman, G. M. M., Shah, S., Richter, R. C., Link, D. D., & Bhandari, S. (2003). Speciation of mercury in soil and sediment by selective solvent and acid extraction. *Analytical and Bioanalytical Chemistry*, *375*(3), 428-436. https://doi.org/10.1007/s00216-002-1701-4

Huggins, F. E., Yap, N., & Huffman, G. P. (1999). XAFS Investigation of Mercury Sorption on Carbon-based and Other Sorbent Materials. *Japanese Journal of Applied Physics*, *38*(S1), 588. https://doi.org/10.7567/jjaps.38s1.588

Huggins, F. E., Yap, N., Huffman, G. P., & Senior, C. L. (2003). XAFS characterization of mercury captured from combustion gases on sorbents at low temperatures. *Fuel Processing Technology*, *82*(2-3), 167-196. https://doi.org/10.1016/s0378-3820(03)00068-7

Kim, C. S., Bloom, N. S., Rytuba, J. J., & Brown, G. E. (2003). Mercury Speciation by X-ray Absorption Fine Structure Spectroscopy and Sequential Chemical Extractions: A Comparison of Speciation Methods. *Environmental Science & Technology*, *37*(22), 5102-5108. https://doi.org/10.1021/es0341485

Kim, C. S., Rytuba, J. J., & Brown, G. E. (2004). Geological and anthropogenic factors influencing mercury speciation in mine wastes: an EXAFS spectroscopy study. *Applied Geochemistry*, *19*(3), 379-393. https://doi.org/10.1016/s0883-2927(03)00147-1

Leonard I. Sweet, J. T. Z. (2001). TOXICOLOGY AND IMMUNOTOXICOLOGY OF MERCURY: A COMPARATIVE REVIEW IN FISH AND HUMANS. *Journal of Toxicology and Environmental Health, Part B*, *4*(2), 161-205. https://doi.org/10.1080/10937400117236

Liu, X., Wang, S., Zhang, L., Wu, Y., Duan, L., & Hao, J. (2013). Speciation of mercury in FGD gypsum and mercury emission during the wallboard production in China. *Fuel*, *111*, 621-627. https://doi.org/10.1016/j.fuel.2013.03.052

Liu, Z., Li, C., Sriram, V., Lee, J.-Y., & Brewe, D. (2016). XANES study of elemental mercury oxidation over RuO2/TiO2 and selective catalytic reduction catalysts for mercury emissions control. *Fuel Processing Technology*, *153*, 156-162. https://doi.org/10.1016/j.fuproc.2016.07.018

López-Antón, M. A., Díaz-Somoano, M., Ochoa-González, R., & Martínez-Tarazona, M. R. (2012). Analytical methods for mercury analysis in coal and coal combustion by-products. *International Journal of Coal Geology*, *94*, 44-53. https://doi.org/10.1016/j.coal.2012.01.010

Sakusabe, K., Kato, T., Okawa, H., & Sugawara, K. (2019). Mercury Forms in By-Products from Coal-Fired Power Plant. *Journal of Chemical Engineering of Japan*, *52*(11), 859-865. https://doi.org/10.1252/jcej.19we002

Sakusabe, K., Kato, T., Okawa, H., & Sugawara, K. (2020). Mercury Forms Contained in Desulfurization Gypsums. *Journal of Chemical Engineering of Japan*, *53*(7), 359-365. https://doi.org/10.1252/jcej.19we213

Scheuhammer, A. M., & Sandheinrich, M. B. (2008). Recent advances in the toxicology of methylmercury in wildlife. *Ecotoxicology*, *17*(2), 67-68. https://doi.org/10.1007/s10646-007-0186-5

Scientific, T. F. (2019). *What you need to know about mercury emissions, regulations, and monitoring* https://assets.thermofisher.com/TFS-Assets/CAD/Handbooks/mercury-emissions-regulations-monitoring-ebook.pdf# (https://assets.thermofisher.com/TFS-Assets/CAD/Handbooks/mercury-emissions-regulations-monitoring-ebook.pdf#)

Semionov, A. (2018). Minamata Disease—Review. *World Journal of Neuroscience*, *08*(02), 178-184. https://doi.org/10.4236/wjns.2018.82016

Streets, D. G., Lu, Z., Levin, L., Ter Schure, A. F. H., & Sunderland, E. M. (2018). Historical releases of mercury to air, land, and water from coal combustion. *Sci Total Environ*, *615*, 131-140. https://doi.org/10.1016/j.scitotenv.2017.09.207

Streets, D. G., Zhang, Q., & Wu, Y. (2009). Projections of Global Mercury Emissions in 2050. *Environmental Science & Technology*, *43*(8), 2983-2988. https://doi.org/10.1021/es802474j

Sugawara, K., Enda, Y., Kato, T., Sugawara, T., & Shirai, M. (2003). Effect of Hydrogen Sulfide on Organic Sulfur Behavior in Coal and Char during Heat Treatments. *Energy & Fuels*, *17*(1), 204-209. https://doi.org/10.1021/ef020161j

Sundseth, K., Pacyna, J. M., Pacyna, E. G., Pirrone, N., & Thorne, R. J. (2017). Global Sources and Pathways of Mercury in the Context of Human Health. *Int J Environ Res Public Health*, *14*(1). https://doi.org/10.3390/ijerph14010105

Uaciquete, D. L. E., Sakusabe, K., Kato, T., Okawa, H., Sugawara, K., & Nonaka, R. (2021). Influence of unburned carbon on mercury chemical forms in fly ash produced from a coal-fired power plant. *Fuel*, *300*. https://doi.org/10.1016/j.fuel.2021.120802

Yang, L., Zhang, Y., Wang, F., Luo, Z., Guo, S., & Strähle, U. (2020). Toxicity of mercury: Molecular evidence. *Chemosphere*, *245*, 125586. https://doi.org/10.1016/j.chemosphere.2019.125586

Zhu, Z., Zhuo, Y., Fan, Y., & Wang, Z. (2016). Fate of mercury in flue gas desulfurization gypsum determined by Temperature Programmed Decomposition and Sequential Chemical Extraction. *J Environ Sci (China)*, *43*, 169-176. https://doi.org/10.1016/j.jes.2015.09.011

Chapter 4: Elution behavior of mercury from coal by-products

4.1 Introduction

In recent years, environmental conservation for sustainable development has become a major goal worldwide. The utilization of renewable energy sources, such as solar and wind power, has grown exponentially. However, the stable operation of renewable energy is challenging as its output fluctuates widely depending on natural conditions. Coal-fired power generation is expected to be utilized as a base load for the power source while promoting high efficiency and reducing the environmental load. According to the Aggregation of Electricity Supply Plans published in Japan in 2021, renewable energy will account for 28% of the power supply in 2030, while coal will account for 34% ("Summary of annual supply plan, 2021-," 2021).

When coal burns, harmful trace elements, in addition to sulfur and nitrogen oxides, are released into the gas phase. Mercury, fluorine, bromine, and chlorine are the most volatile elements in coal. Mercury in coal exists in forms of sulfide-bound mercury (mainly pyritic mercury), clay-bound mercury, and organic matter-bound mercury (Zhao et al., 2019), at an average content of about 0.1 ppm (Rallo et al., 2012). Despite its low content, coal is considered one of the main anthropogenic sources of mercury emissions (Sundseth et al., 2017).

Mercury emission from coal-fired power plants into the atmosphere has been extensively reviewed. Mercury emitted in the natural environment can undergo a series of chemical transformations to an organic form, methylmercury (CH_3Hg), which is highly toxic (Counter & Buchanan, 2004; Heckel et al., 2013) and has a substantial impact on human and ecosystem health at local and global scales (Driscoll et al., 2013; Gworek et al., 2017; Lavoie et al., 2013). Thus, implementing strategies, technologies, and regulations to limit the release and exposure to mercury should be emphasized. Coal-fired power plants are fitted with equipment for exhaust gas treatment, such as selective catalytic reduction units (SCR), electrostatic precipitators (EP), and wet desulfurization units (WFGD), in which mercury is captured and recovered with fly ash and gypsum. Such set-ups significantly reduce mercury emissions into the atmosphere. However, as air emission control becomes strict, the partitioning of mercury is found to shift towards non-air releases (Diao et al., 2018; Streets et al., 2018). And with the growing demand for environmental protection, the output of fly ash and flue gas desulfurization gypsum has increased worldwide. In countries such as Japan, the effective use rate of gypsum was almost 100% in 2017 (JCOAL, 2017). The primary use of desulfurization gypsum is in the construction field, as a raw material

for wallboard production (Lei et al., 2017; Liu et al., 2021; Pantini et al., 2019; Pedreño-Rojas et al., 2020; Ye et al., 2019). However, the utilization of fly ash and desulfurization gypsum increases concerns of mercury leaching as the mercury contained in these by-products can be transported into rivers and find its way into lakes and oceans (Amos et al., 2014; Ogawa et al., 2018; Truman et al., 2010). Hence, investigating the leaching potential of mercury from desulfurization gypsum is essential to predict the risk of pollution when gypsum is utilized as the construction material, or when it is finally landfilled. Compared to fly ash, information on the leaching potential of mercury from desulfurization gypsum is limited. Typically, the release potential of heavy metals, including mercury, is predicted using batch or fixed-bed-column leaching systems. Fixed-column leaching may be the most appropriate method for simulating field conditions (Benito, 2001; Kim et al., 2003). However, a fixed column system is ineffective for fine-grained gypsum due to insufficient permeability (Kairies et al., 2006).

In this study, we have attempted to develop an accurate method for evaluating mercury elution from desulfurization gypsum. We achieved this by comparing two types of elution tests: the conventional batch elution and the semi-batch method. The elution behavior was kinetically modeled using the chemical forms of mercury in gypsum.

4.2 Experimental method

4.2.1 Gypsum samples

The two types of gypsum samples used in this study were obtained from a commercial coal-fired power plant. Both samples were collected from a double-contact flow-type desulfurization equipment. Table 4.1 presents the values of total mercury and carbon content. These values depend on the type of coal and combustion conditions. All samples were dried at 100 ℃ for 24 h prior to the analysis. The surface of the gypsum samples was observed using a scanning electron microscope (SEM-EDX, JSM-7800F, JEOL Corp.). Figure 4.1 shows an example of the SEM image of Sample No. 1. Distinct differences were not observed between the features of Samples 1 and 2.

Table 4.1 Composition of desulfurization gypsum samples.

Gypsum	Hg [ppm]	C [wt.%]
No.1	1.10	0.19
No.2	0.70	0.14

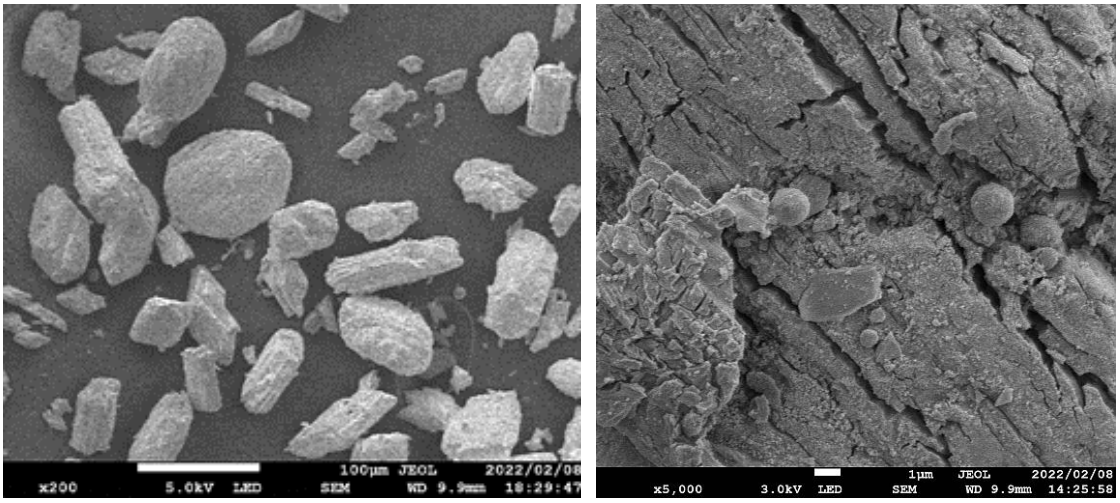

Figure 4.1 SEM photo of gypsum sample No.1.

4.2.2 Elution test using the conventional batch system

To investigate the elution behavior of mercury from gypsums when exposed to rainwater, the elution test was carried out following the conventional batch method described by the Japanese standardized leaching Test No.13 referred by Japan's policy on environmental management of mercury wastes. In this test, 5 g of gypsum was added to 50 ml of deionized water and shaken at 250 rpm for 1 min to 6 h under room temperature. Afterward, the mixture was subjected to solid-liquid separation by filtration through a 0.45 μm membrane filter. The filtrates were preserved by adding 20 mL of 50 g/L $KMnO_4$.

4.2.3 Elution test using the improved semi-batch test

As means to precisely evaluate the amount of Hg eluted at every step of the elution test as well as the time necessary for the dissolution of mercury to reach a steady state, an improved semi-batch method was designed. Here, the mixing ratio of the gypsum sample and solution was set to a weight ratio of 1:3. The mixture was thoroughly stirred, and samples of the eluate were collected every 10 min in a total time of 160 min. Other conditions such as pH, temperature, and stirring speed were maintained similar to those described in the conventional method.

4.2.4 Elemental analysis

Carbon contents in all samples were quantified using an NCH analyzer (Sumika Chemical Analysis Service, NCH-22A). The surface of was observed using a scanning electron microscope (SEM-EDX, JSM-7800F, JEOL Corp.). And the chemical forms of mercury in gypsum were identified and quantified by combining temperature-programmed desorption and cold vapor atomic adsorption spectrophotometry (TPD-CVAAS) (Sakusabe et al., 2019, 2020). The schematic of the system is shown in Figure 4.2. The sample was heated in an electric furnace to 700 °C at a heating rate of 5 °C/min in an argon gas stream of 250 ml/min. Mercury compounds were desorbed from the sample, and the generated mercury compound vapor was bubbled into a stannic chloride solution of 90 g/mL, where mercury was reduced to elemental mercury.

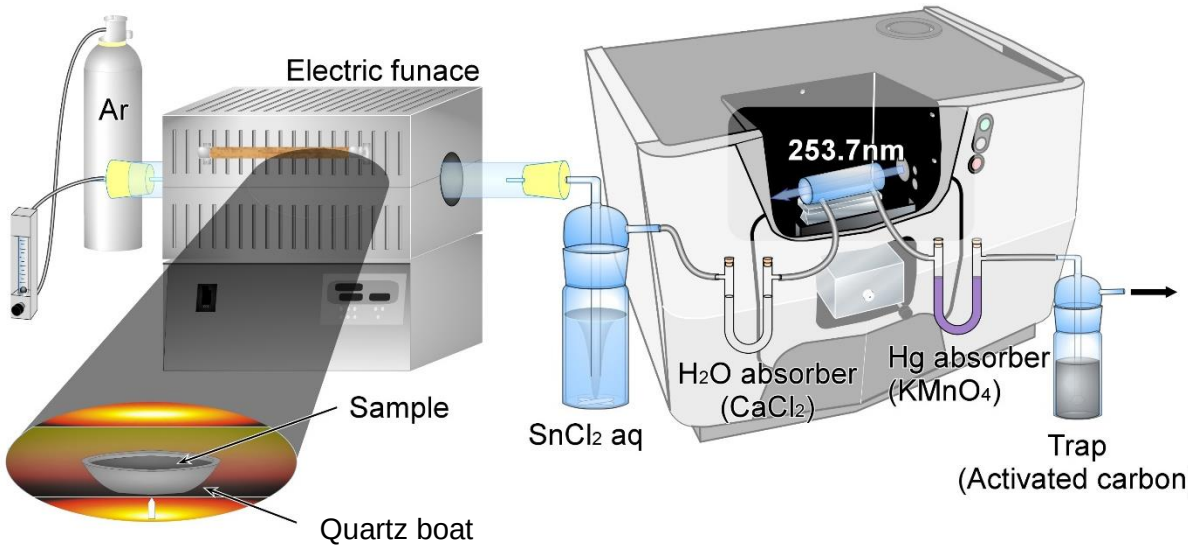

Figure 4.2 Schematic diagram of the Hg thermos-desorption and CVAAS apparatus for mercury speciation according to Sakusabe K. *et al.*, 2020.

Subsequently, it passed through a water absorption tube of calcium chloride, and atomic absorption was measured with an atomic absorption spectrophotometer installed on the downstream side of the equipment.

The chemical form analysis of mercury was performed by linearly combining the TPD curves of various model mercury compounds and simulating the TPD curve of the sample using the least squares method with the abundance ratio of each form as a parameter. According to Sakusabe *et al.* [24, 25], mercury exists in a state bound to chlorine, sulfur, and oxygen depending on the flue gas or desulfurization equipment conditions. Five types of mercury compounds, Hg_2Cl_2, $HgCl_2$, HgO, HgS, $HgSO_4 \cdot 2HgO$, and $HgSO_4$, were prepared by mixing Hg_2Cl_2 (EP, Wako Pure Chemicals), HgO (GR, Nacalai Tesque), HgS (GR, Kanto Chemical), $HgSO_4$ (GR, Wako Pure Chemicals) with silicon dioxide (GR, Nacalai Tesque), and calcium sulfate dihydrate. The mercury content of all the model samples was adjusted to 10 ppm.

In addition, considering the possibility that mercury may be adsorbed by unburned carbon mixed in desulfurization gypsum, and that the unburned carbon in FGD gypsum is exposed to reactive gases such as HCl and SO_2 in flue gas, it can change the surface condition and affect mercury

adsorption (Wu et al., 2015). Carbon with adsorbed mercury was also prepared as a model sample. The carbon used for the preparation was bituminous coal-based activated carbon (GR, Nacalai Tesque, Inc.) and unburned carbon (UC) separated from fly ash generated at a coal-fired power plant. Activated carbon (AC) or UC was soaked in an aqueous solution containing dissolved HgO for one hour to prepare carbon with adsorbed mercury (AC-Hg and UC-Hg).

The mercury in the filtrate was quantified using a cold vapor atomic absorption spectrophotometer (AA-7000, Shimadzu Corp.) using $HONH_3Cl$ to reduce excess $KMnO_4$ and $SnCl_2$ as a reduction agent.

In addition, quantification of mercury in the filtrate was carried by Cold Vapor Atomic Absorption Spectrophotometer (AA-7000, Shimadzu Corp.) by using $HONH_3Cl$ to reduce the excess of $KMnO_4$ and $SnCl_2$ as a reduction agent.

4.3 Results and discussion

4.3.1 Elution behavior of mercury in the batch method

The elution behavior of mercury in the batch system was also investigated. The leaching conditions were maintained as described in the standard test, and the leaching time was varied from 1 min to 6 h. Figures 4.3 and 4.4 show the change in dissolved mercury C_R (μg-Hg/g-gypsum) as a function of time. Rapid dissolution of mercury was observed during the first stage of the elution test for both samples. Gypsum No. 1 achieved an elution peak of mercury after 30 min of elution. Gypsum no. 2 reached its peak after 60 min. However, after reaching the elution peak, the mercury content of the liquid gradually decreased. Therefore, it is difficult to precisely evaluate the amount of mercury eluted in the elution test. The shapes of the dissolution profiles suggest that the initial ascending shape of the curves indicates a rapid dissolution of mercury into the solution, and the curve descends after the elution peak may be caused by the adsorption of mercury by gypsum. Mercury tends to be associated with sulfur and chlorine (Z. Li, 2002). In this case, mercury adsorption on gypsum is thought to be a result of interactions between minor elements such as chlorine and sulfur-containing functional groups available in the unburned carbon (Sun et al., 2017; Uaciquete et al., 2021; Wajima & Sugawara, 2011). An improved method should be designed to prevent adsorption and precisely evaluate the elution potential of mercury from desulfurization gypsum.

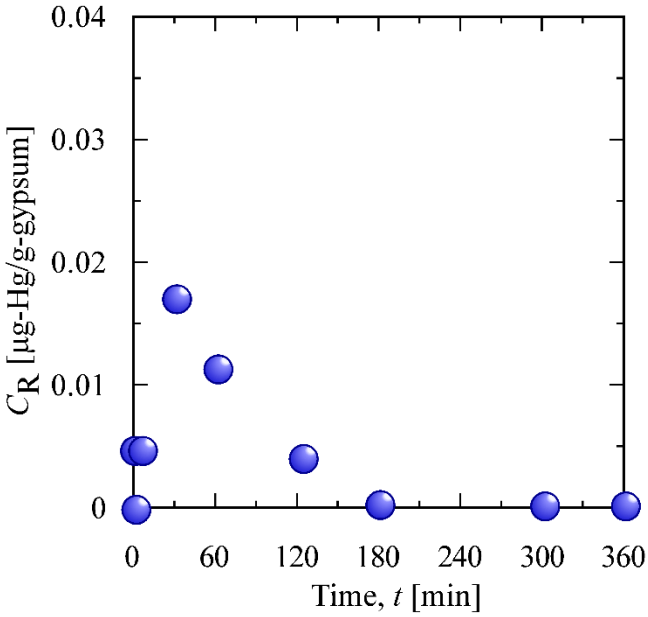

Figure 4.3 Change in dissolved Hg with time in batch elution experiment of gypsum No. 1.

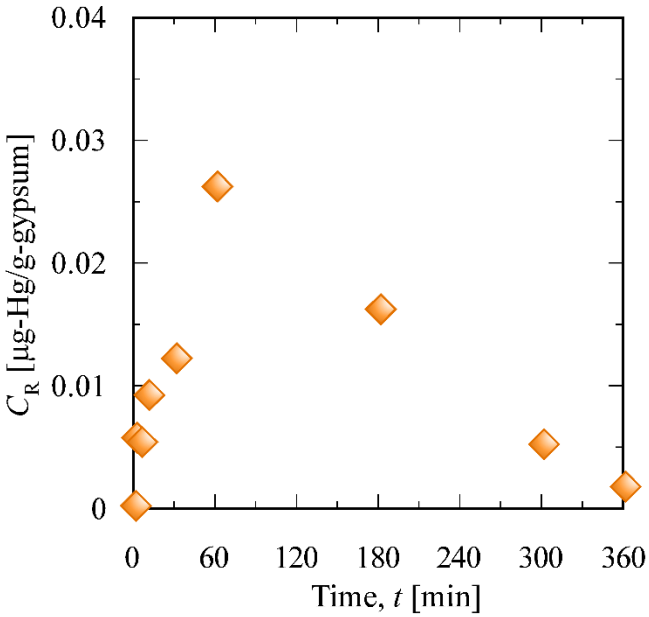

Figure 4.4 Change in dissolved Hg with time in batch elution experiment of gypsum No. 2.

4.3.2 Elution behavior of mercury in the semi-batch method

A semi-batch test was designed to determine the precise amount of mercury dissolvable from gypsum. The mixing ratio of the gypsum sample and solution was set to a weight ratio of 1:3. The mixture was thoroughly stirred, and samples of the eluate were collected every 10 min for a total time of 180 min. At the same time, other conditions, such as temperature and stirring speed, were maintained similar to those described in the conventional batch method. Figures 4.5 and 4.6 show the extent of mercury elution as a function of time. Contrary to the batch test results, the elution behavior showed that the influence of adsorption was negligible. The mercury elution for all samples rapidly increased with time, and the maximum dissolution amount was obtained after 60 min of leaching.

If the adsorption of mercury by gypsum can be neglected in the batch experiment, the possible mercury concentrations were estimated to be 0.035 ppm and 0.038 ppm in the water for gypsum samples 1 and 2, respectively, according to the observed maximum elution amount in the semi-batch experiments. These estimated values exceeded the effluent standard of mercury 0.005 ppm as shown in Figure 4.7. It is possible to release mercury beyond the effluent standard when desulfurization gypsum is placed in the water flow system.

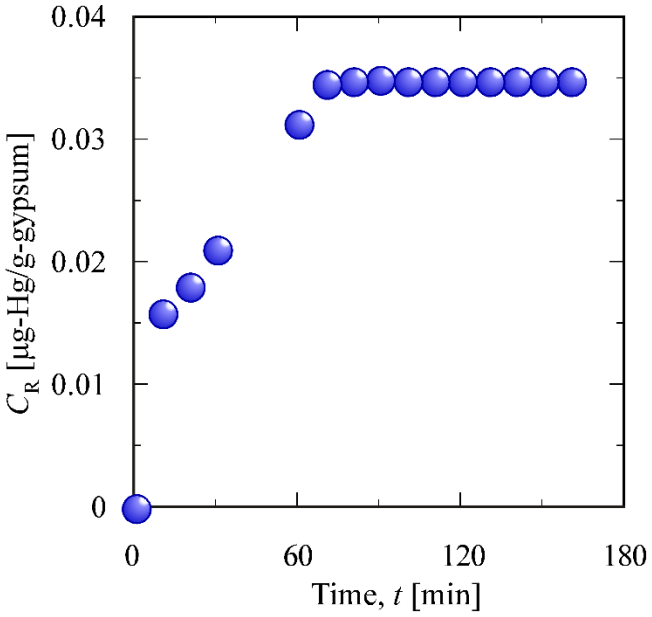

Figure 4.5 Change in dissolved Hg with time in semi-batch elution experiment of gypsum No. 1.

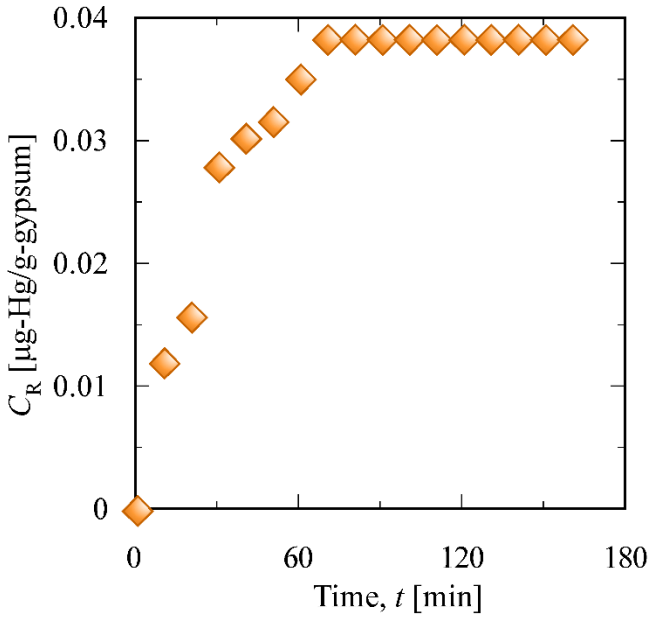

Figure 4.6 Change in dissolved Hg with time in semi-batch elution experiment of gypsum No. 2.

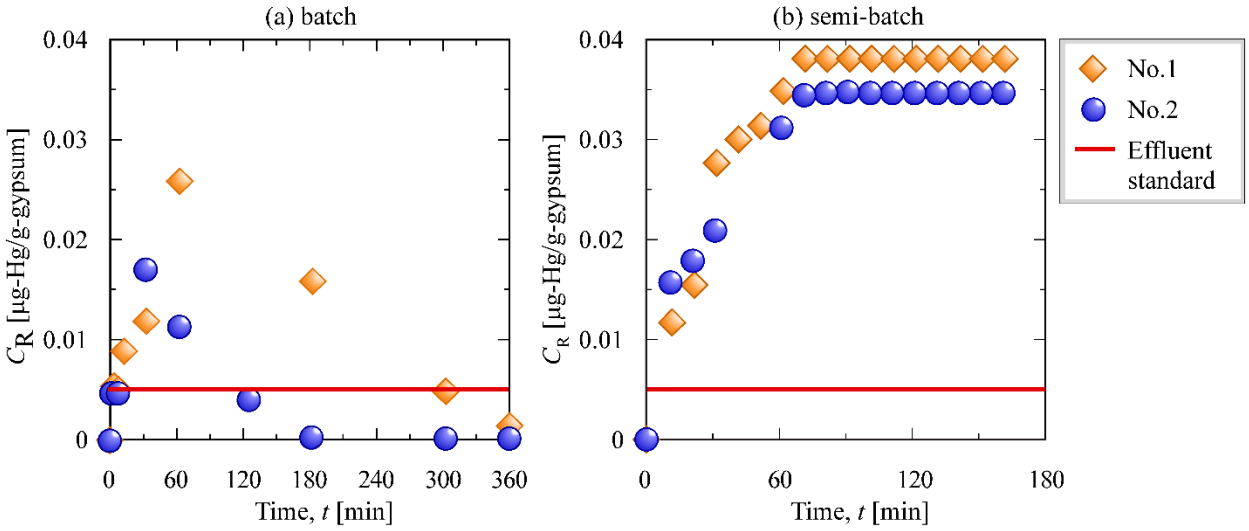

Figure 4.7 Comparison of mercury concentration in the solution from the elution tests and the mercury effluent standard

4.3.4 Chemical mercury forms in the gypsum samples

Figure 4.8 shows the TPD curves of mercury in the desulfurization gypsum samples. The rhombic key represents the observed data. The black solid lines indicate the fitted values obtained from the linear combination of the TPD curves for the mercury model compounds. Table 4.2 shows the abundance ratios of mercury forms determined by the simulation. TPD profiles of both No. 1 and No. 2 showed a peak position at approximately 280 °C, confirming that both samples contained carbon-associated mercury forms of UC-Hg and AC-Hg. Unburned carbon (UC) and activated carbon (AC) are derived from bituminous coal, but AC is formed through steam activation at high temperatures, whereas UC is formed by exposing unburned particles to reactive gases such as HCl and SO_2. Therefore, the surface functional groups were clearly different. Oxygen functional groups, such as ester and carbonyl groups of activated carbon, are involved in mercury adsorption (Sun et al., 2017). Table 4.2 shows that carbon-associated UC-Hg is the main chemical form of mercury ranging from 75% to 94% for gypsum No. 1 and No. 2, respectively.

Figure 4.9 shows the TPD curves of gypsum obtained after the elution tests. The determined abundance ratios of the mercury forms are listed in Table 4.3.

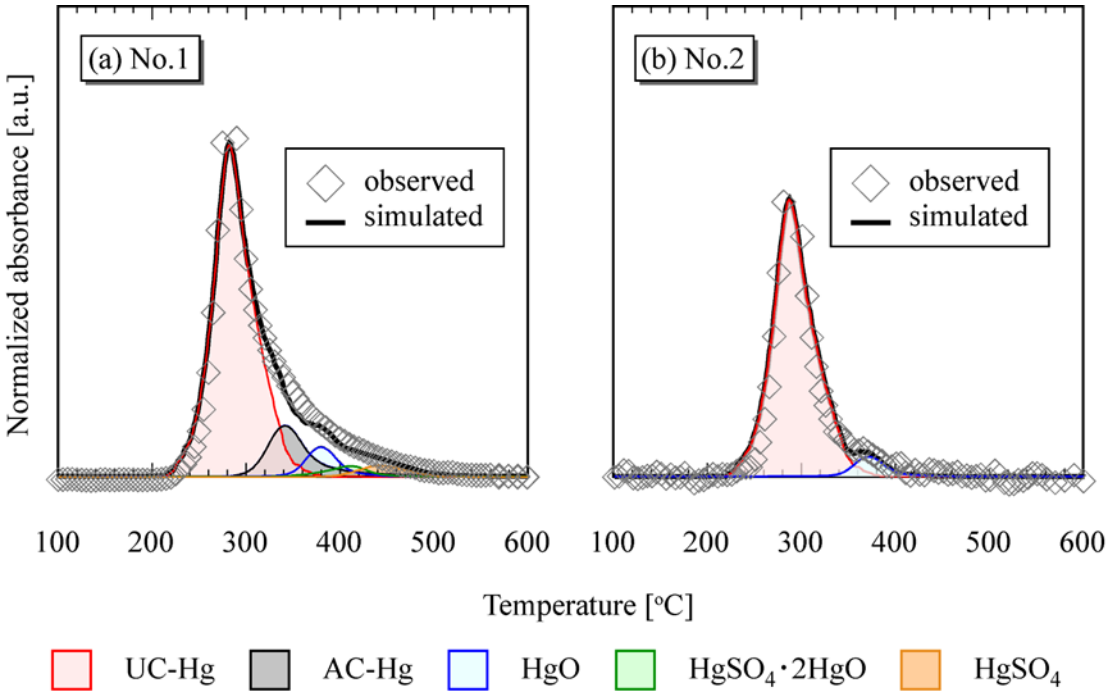

Figure 4.8 TPD curves and fitting results of gypsum samples (a) No.1 and (b) No.2.

Table 4.2 Abundance ratio of mercury forms in the gypsum raw samples.

Sample	Abundance ratio of Hg forms [%]					
	UC-Hg	AC-Hg	HgO	HgS	$HgSO_4.2HgO$	$HgSO_4$
No.1	75	13	6	3	3	0
No.2	94	0	6	0	0	0

The eluted amount was less than 5% of the total mercury content in gypsum; therefore, a distinct change was not observed in the TPD curves before and after elution. While the precise interpretation of mercury forms involves difficulties, it was confirmed that the semi-batch samples of both No. 1 and 2 contained only UC-Hg and AC-Hg. This resulted from the fact that all soluble mercury was removed from the gypsum in the semi-batch method. In the batch method, all mercury existed in carbon-associated forms after the elution test. This implies that soluble mercury was transformed into stable carbon-associated forms during adsorption.

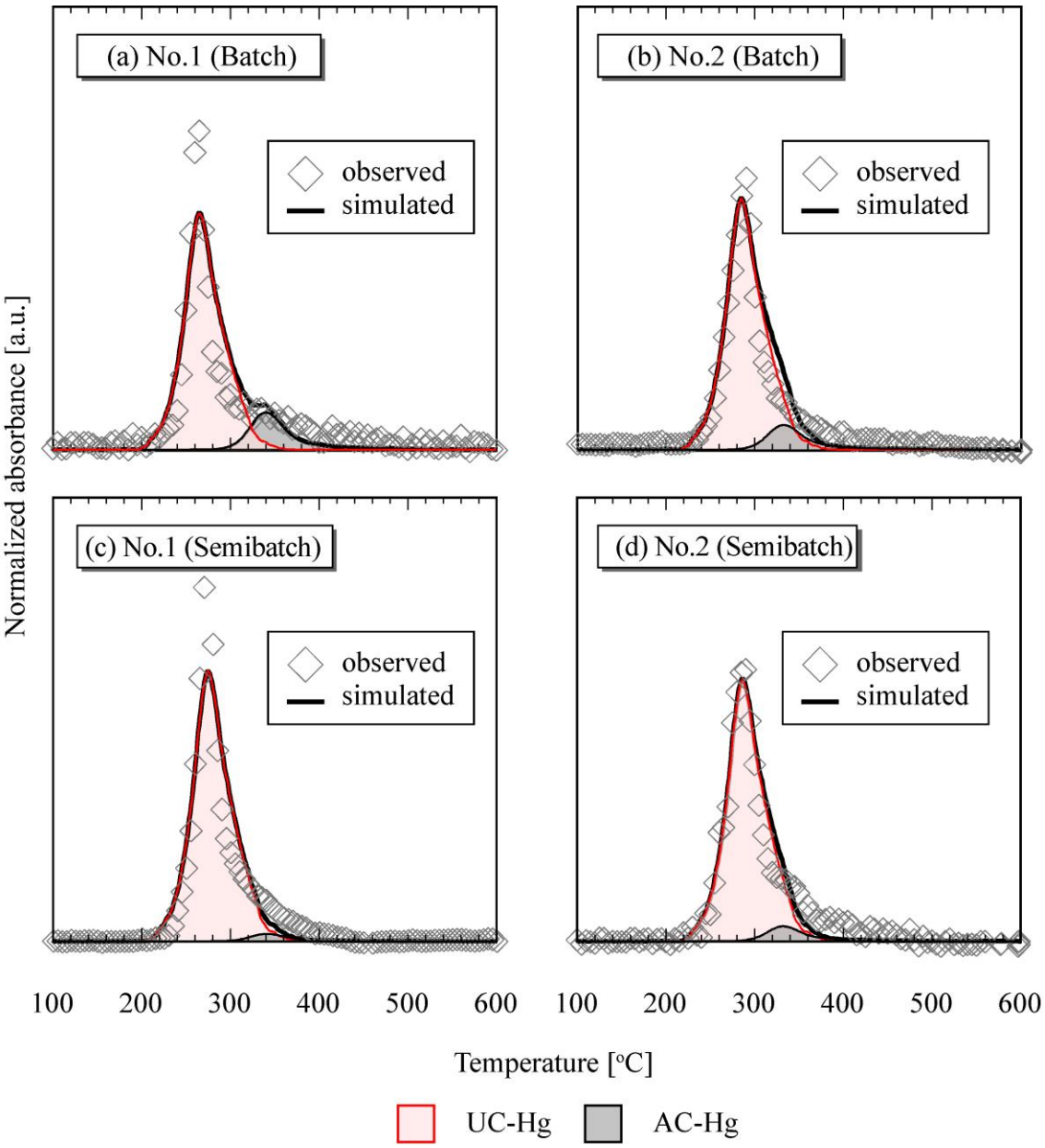

Figure 4.9 TPD curves and fitting results of gypsum samples after elution tests (a) No.1 in batch system, (b) No.2 in batch system, (c) No.1 in semi-batch system and (d) No.2 in semi-batch system.

Table 4.3 Abundance ratio of mercury form in gypsum before and after elution tests [% of total Hg in sample].

Sample	Elution system	UC-Hg	AC-Hg	HgO	HgS	$HgSO_4 \cdot 2HgO$	$HgSO_4$
No.1	-	75	13	6	3	3	0
	Batch	85	15	0	0	0	0
	Semi-batch	97	3	0	0	0	0
No.2	-	94	0	6	0	0	0
	Batch	90	10	0	0	0	0
	Semi-batch	94	6	0	0	0	0

4.3.5 Rate analysis of elution

Mercury eluted from gypsum to distilled water was adsorbed by gypsum in the batch method. The maximum dissolution amount of mercury existed in the semi-batch method. Here, we assume the following series of reactions.

$$A \rightarrow R \rightarrow S$$

A, R, and S represent soluble mercury in gypsum, eluted mercury in water, and mercury re-adsorbed by gypsum, respectively as shown in Figure 4.10. Assuming that the first-order reaction of mercury content expresses the elution and re-adsorption rates, the material balance equations (7–11) are expressed as follows:

$$dX_A/dt = -k_1 X_A \quad (7)$$

$$dX_R/dt = k_1 X_A - k_2 X_R \quad (8)$$

$$dX_S/dt = k_2 X_R \quad (9)$$

$$X_A + X_R + X_S = X_{A0} \quad (10)$$

$$X_A = X_{A0},\ X_R = X_S = 0 \text{ at } t = 0 \quad (11)$$

k_1 and k_2 are the rate constants of elution and re-adsorption, respectively. X_A, X_R, and X_S show the extent of mercury in the gypsum phase, eluted mercury in the water phase, and re-adsorbed

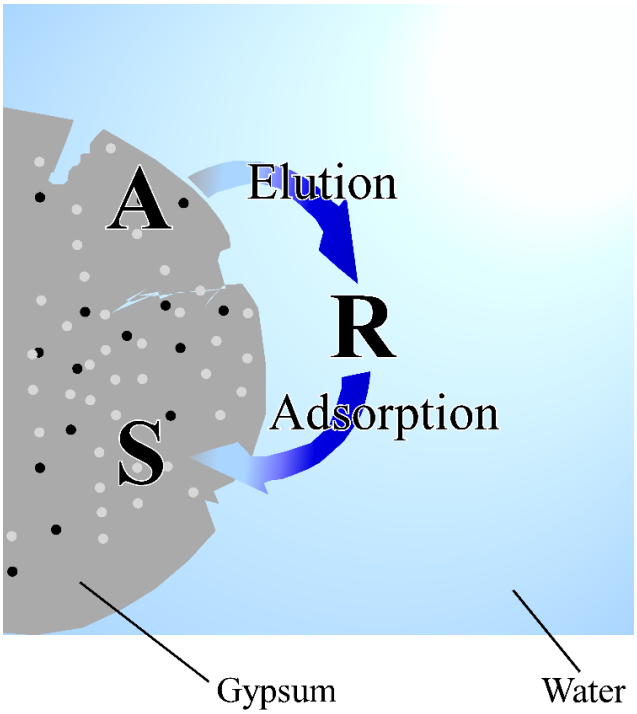

Figure 4.10 Elution behavior of mercury from gypsum.

mercury in the gypsum phase, respectively. X_{A0} is the maximum amount of soluble mercury determined using the semi-batch method.

The solid lines in Figures 4.11 and 4.12 represent the simulated values and express the change in the amount of eluted mercury, showing the maximum values. Figures 4.13 and 4.14 show the simulated curves of elution behavior of mercury using the semi-batch method as solid lines. The determined rate constants and the maximum extent of elution are listed in Table 4.4.

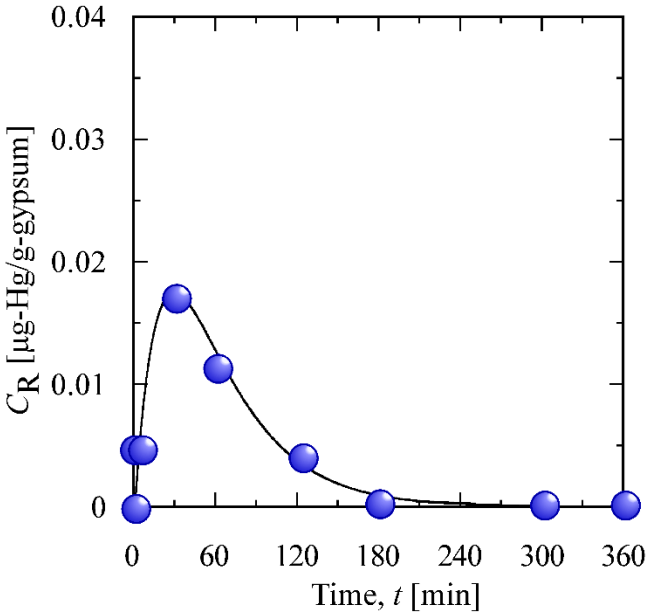

Figure 4.11 Change in dissolved Hg with time in batch elution experiment of gypsum No. 1. The solid line shows the experimental and simulated values.

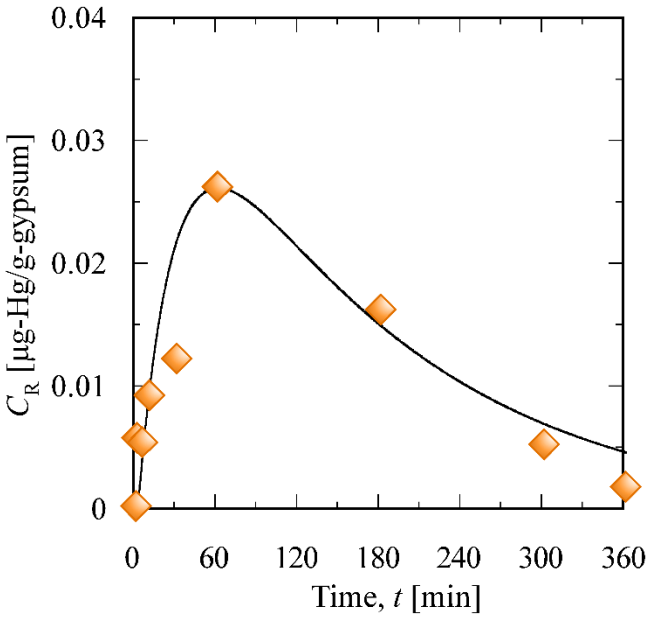

Figure 4.12 Change in dissolved Hg with time in batch elution experiment of gypsum No. 2. The solid line shows the experimental and simulated values.

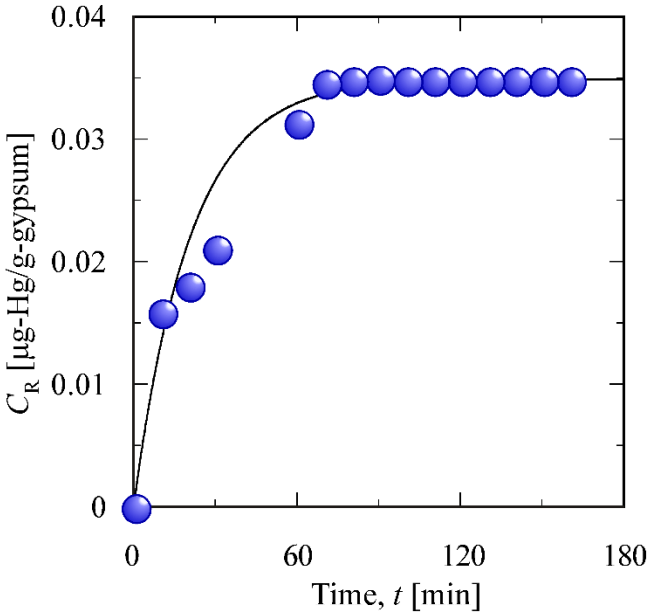

Figure 4.13 Change in dissolved Hg with time in semi-batch elution experiment of gypsum No. 1. The solid line shows the experimental and simulated values.

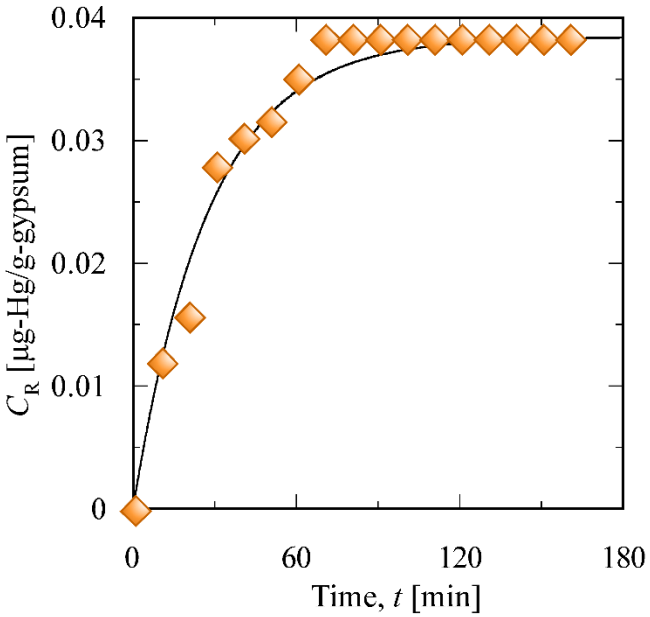

Figure 4.14 Change in dissolved Hg with time in semi-batch elution experiment of gypsum No. 2. The solid line shows the experimental and simulated values.

Table 4.4 Rate constants for elution and re-adsorption of mercury from gypsum.

Gypsum samples	Rate constants		Extent of Hg elution [%]
	k_1 [s^{-1}]	k_2 [s^{-1}]	
No. 1	8.0×10^{-4}	4.0×10^{-4}	3.2
No. 2	6.0×10^{-4}	1.0×10^{-4}	5.5

The rate constants of the elution of mercury k_1 from both gypsums were similar. However, the rate constant of adsorption k_2 of Sample No. 1 was four times larger than that of Sample No. 2, which might be related to the carbon content in the gypsum. Most of the mercury in the fly ash and desulfurization gypsum produced from coal-fired plants exists in unburned carbon in the form of sulfur-, chlorine-, and oxygen-related compounds (Uaciquete et al., 2021). In particular, sulfur has a strong affinity for mercury. The adsorption of mercury by gypsum in the present batch experiments implied that the eluted mercury formed a stable compound with sulfur contained in the unburned carbon. Wajima and Sugawara reported mercury adsorption using pyrolyzed coal with and without sulfur impregnation (Wajima & Sugawara, 2011). Sulfur impregnation increased the amount of adsorbed mercury. The mercury adsorption rate constant for the sulfur-impregnated coal showed 10^{-4} s^{-1} order assuming a first-order reaction. This kinetic value was similar to the re-adsorption rate in the batch experiments.

4.4 Conclusion

Mercury elution from desulfurization gypsum was analyzed using conventional batch tests. In this test, the dissolved mercury was found to readily re-adsorb into gypsum; therefore, the precise amount of mercury could not be evaluated.

In order to evaluate the precise amount of mercury from desulfurization gypsums, an improved semi-batch system was designed. Here, the adsorption phenomenon was negligible, and it was confirmed that the dissolved mercury concentration in both samples exceeded the effluent standard. Changes in mercury forms before and after the elution tests were analyzed using a combination of Temperature Programmed Desorption and Cold Vapor Atomic Absorption Spectroscopy. It was demonstrated that, in the batch test, the soluble mercury was later transformed into more stable carbon-associated forms for both types of gypsum. In contrast, all the soluble mercury was removed after the elution test in the semi-batch tests. Thus, the semi-batch test is a more accurate for evaluating and predicting the risk of mercury elution from desulfurization gypsum.

References

Amos, H. M., Jacob, D. J., Kocman, D., Horowitz, H. M., Zhang, Y., Dutkiewicz, S., Horvat, M., Corbitt, E. S., Krabbenhoft, D. P., & Sunderland, E. M. (2014). Global biogeochemical implications of mercury discharges from rivers and sediment burial. *Environ Sci Technol*, *48*(16), 9514-9522. https://doi.org/10.1021/es502134t

Benito, Y. (2001). Study of leaches obtained from the disposal of fly ash from PFBC and AFBC processes. *Chemical Engineering Journal*, *84*(2), 167-171. https://doi.org/10.1016/s1385-8947(01)00201-7

Counter, S. A., & Buchanan, L. H. (2004). Mercury exposure in children: a review. *Toxicol Appl Pharmacol*, *198*(2), 209-230. https://doi.org/10.1016/j.taap.2003.11.032

Diao, X., Yuan, C.-G., Wu, J., Zhang, K., Zhang, C., & Gui, B. (2018). Mercury fractions in gypsum and estimation of mercury emission from coal-fired power plants. *Fuel*, *226*, 298-306. https://doi.org/10.1016/j.fuel.2018.04.002

Driscoll, C. T., Mason, R. P., Chan, H. M., Jacob, D. J., & Pirrone, N. (2013). Mercury as a global pollutant: sources, pathways, and effects. *Environ Sci Technol*, *47*(10), 4967-4983. https://doi.org/10.1021/es305071v

Gworek, B., Dmuchowski, W., Baczewska, A. H., Bragoszewska, P., Bemowska-Kalabun, O., & Wrzosek-Jakubowska, J. (2017). Air Contamination by Mercury, Emissions and Transformations-a Review. *Water Air Soil Pollut*, *228*(4), 123. https://doi.org/10.1007/s11270-017-3311-y

Heckel, P. F., Keener, T. C., & LeMasters, G. K. (2013). Background Soil Mercury: An Unrecognized Source of Blood Mercury in Infants? *Open Journal of Soil Science*, *03*(01), 23-29. https://doi.org/10.4236/ojss.2013.31004

JCOAL. (2017). *Coal Ash National survey Report*.

Kairies, C., Schroeder, K., & Cardone, C. (2006). Mercury in gypsum produced from flue gas desulfurization. *Fuel*, *85*(17-18), 2530-2536. https://doi.org/10.1016/j.fuel.2006.04.027

Kim, A. G., Kazonich, G., & Dahlberg, M. (2003). Relative Solubility of Cations in Class F Fly Ash. *Environmental Science & Technology*, *37*(19), 4507-4511. https://doi.org/10.1021/es0263691

Lavoie, R. A., Jardine, T. D., Chumchal, M. M., Kidd, K. A., & Campbell, L. M. (2013). Biomagnification of Mercury in Aquatic Food Webs: A Worldwide Meta-Analysis. *Environmental Science & Technology*, *47*(23), 13385-13394. https://doi.org/10.1021/es403103t

Lei, D.-Y., Guo, L.-P., Sun, W., Liu, J.-p., & Miao, C.-w. (2017). Study on properties of untreated FGD gypsum-based high-strength building materials. *Construction and Building Materials*, *153*, 765-773. https://doi.org/10.1016/j.conbuildmat.2017.07.166

Liu, S., Liu, W., Jiao, F., Qin, W., & Yang, C. (2021). Production and resource utilization of flue gas desulfurized gypsum in China - A review. *Environ Pollut*, *288*, 117799. https://doi.org/10.1016/j.envpol.2021.117799

Ogawa, Y., Sakakibara, K., Seki, T., & Inoue, C. (2018). Immobilization of Boron and Arsenic in Alkaline Coal Fly Ash through an Aging Process with Water and Elucidation of the Immobilization Mechanism. *Water, Air, & Soil Pollution*, *229*(11). https://doi.org/10.1007/s11270-018-3997-5

Pantini, S., Giurato, M., & Rigamonti, L. (2019). A LCA study to investigate resource-efficient strategies for managing post-consumer gypsum waste in Lombardy region (Italy). *Resources, Conservation and Recycling*, *147*, 157-168. https://doi.org/10.1016/j.resconrec.2019.04.019

Pedreño-Rojas, M. A., De Brito, J., Flores-Colen, I., Pereira, M. F. C., & Rubio-de-Hita, P. (2020). Influence of gypsum wastes on the workability of plasters: Heating process and microstructural analysis. *Journal of Building Engineering*, *29*. https://doi.org/10.1016/j.jobe.2019.101143

Rallo, M., Heidel, B., Brechtel, K., & Maroto-Valer, M. M. (2012). Effect of SCR operation variables on mercury speciation. *Chemical Engineering Journal*, *198-199*, 87-94. https://doi.org/10.1016/j.cej.2012.05.080

Sakusabe, K., Kato, T., Okawa, H., & Sugawara, K. (2019). Mercury Forms in By-Products from Coal-Fired Power Plant. *Journal of Chemical Engineering of Japan*, *52*(11), 859-865. https://doi.org/10.1252/jcej.19we002

Sakusabe, K., Kato, T., Okawa, H., & Sugawara, K. (2020). Mercury Forms Contained in Desulfurization Gypsums. *Journal of Chemical Engineering of Japan*, *53*(7), 359-365. https://doi.org/10.1252/jcej.19we213

Streets, D. G., Lu, Z., Levin, L., Ter Schure, A. F. H., & Sunderland, E. M. (2018). Historical releases of mercury to air, land, and water from coal combustion. *Sci Total Environ*, *615*, 131-140. https://doi.org/10.1016/j.scitotenv.2017.09.207

Summary of annual supply plan, 2021-. (2021). In J. Organization for Cross-regional Coordination of Transmission Operators (Ed.), *Aggregation of Electricity Supply Plans for FY2021*. Japan.

Sun, P., Zhang, B., Zeng, X., Luo, G., Li, X., Yao, H., & Zheng, C. (2017). Deep study on effects of activated carbon's oxygen functional groups for elemental mercury adsorption using temperature programmed desorption method. *Fuel*, *200*, 100-106. https://doi.org/10.1016/j.fuel.2017.03.031

Sundseth, K., Pacyna, J. M., Pacyna, E. G., Pirrone, N., & Thorne, R. J. (2017). Global Sources and Pathways of Mercury in the Context of Human Health. *Int J Environ Res Public Health*, *14*(1). https://doi.org/10.3390/ijerph14010105

Truman, C. C., Nuti, R. C., Truman, L. R., & Dean, J. D. (2010). Feasibility of using FGD gypsum to conserve water and reduce erosion from an agricultural soil in Georgia. *Catena*, *81*(3), 234-239. https://doi.org/10.1016/j.catena.2010.04.003

Uaciquete, D. L. E., Sakusabe, K., Kato, T., Okawa, H., Sugawara, K., & Nonaka, R. (2021). Influence of unburned carbon on mercury chemical forms in fly ash produced from a coal-fired power plant. *Fuel*, *300*. https://doi.org/10.1016/j.fuel.2021.120802

Wajima, T., & Sugawara, K. (2011). Adsorption behaviors of mercury from aqueous solution using sulfur-impregnated adsorbent developed from coal. *Fuel Processing Technology*, *92*(7), 1322-1327. https://doi.org/10.1016/j.fuproc.2011.02.008

Wu, S.-j., Katayama, R., Azhar Uddin, M., Sasaoka, E., & Xie, Z.-m. (2015). Study on Reactivity of HgO over Activated Carbon with HCl and SO2 in the Presence of Moisture by Temperature-Programmed Decomposition Desorption Mass Spectrometry. *Energy & Fuels*, *29*(10), 6598-6604. https://doi.org/10.1021/acs.energyfuels.5b01283

Ye, J., Zubair, M., Wang, S., Cai, Y., & Zhang, P. (2019). Power production waste. *Water Environment Research*, *91*(10), 1091-1096. https://doi.org/10.1002/wer.1200

Z. Li, X. S., J. Luo, J. Y. Hwang. (2002). Unburned carbon from fly ash for mercury adsorption II. Adsorption isotherms and mechanisms. *Journal of mineral and Materials characterization and Engineering*, *1*, 79-96.

Zhao, S., Pudasainee, D., Duan, Y., Gupta, R., Liu, M., & Lu, J. (2019). A review on mercury in coal combustion process: Content and occurrence forms in coal, transformation, sampling methods, emission and control technologies. *Progress in Energy and Combustion Science*, *73*, 26-64. https://doi.org/10.1016/j.pecs.2019.02.001

Chapter 5: Summary

In this study we focused on coal cleaning technologies as well as the efficient utilization of coal combustion by-products. Which are undeniably crucial topics related to the efforts in minimization of the environmental impacts of coal utilization.

The study has demonstrated a new option for removal of sulfur from coal prior to the utilization. In addition, a contribution to the understanding of mercury speciation and fate during coal utilization, was made by demonstrating the influence of unburned carbon in the mercury forms in fly ash as well as the elution behavior of mercury from desulfurization gypsum.

Chapter 1 outlines some background information and general aspects in recent trends on coal utilization and coal cleaning technologies including high efficiency energy generation technologies such as integrated gasification combined cycle (IGCC). Furthermore, given the fact that currently used desulfurization methods prior to combustion which include mainly physical methods such as flotation and magnetic separation are not effective to remove organic sulfur, chemical-based desulfurization methods are becoming more attractive. In addition, as the global regulation of mercury emissions becomes more stringent each year, the issues of concern of utilization of coal combustion by-products were clarified. And the aim and objectives of this study were also described.

In chapter 2, a selective oxidation process that can be performed under mild conditions with high carbon yield, was developed by using peracetic acid. Sulfur forms in the raw and treated coals were accurately specified by Sulfur K-edge X-ray absorption near edge structure analysis (XANES). It was confirmed that by peracetic acid, a selective organic sulfur removal from subbituminous coal is achieved at room temperature. Peracetic acid showed good performance for thiophenic sulfur conversion. Thiophene was converted into its oxidized sulfone form which was then removed by thermal treatment at 400 °C maintaining a high carbon yield of about 90%.

In chapter 3, as an effort to understand the relation between the mercury forms and the unburned carbon contained in fly ash, mercury forms in fly ash with a rich fraction of unburned

carbon were qualitatively and quantitatively analyzed by Hg L_{III}-edge XANES analysis. Estimation of chemical forms of mercury was initially done by an inflection point method. Additionally, qualitative and quantitative analyses were performed by linear combination fitting using XANES spectra of the control mercury compounds. The XANES spectrum of the unburned carbon samples showed that all mercury in fly ash bounds to sulfur, chlorine and oxygen compounds. It was demonstrated the mercury chemical forms in fly ash were remarkably influenced by the presence of sulfur, chlorine and oxygen in the unburned carbon.

In chapter 4, the elution behaviour of mercury from desulfurization gypsum was studied. For the elution test, the conventional batch method and the improved semi-batch were applied. The results revealed that the dissolution behavior of mercury varied significantly with the testing method. It was demonstrated that in a batch system, a sequential phenomenon of elution and adsorption occurs. Initially, Hg from gypsums is rapidly eluted and then gradually adsorbed onto the gypsum surface, and transformed into more stable carbon-associated mercury forms. On the other hand, in the improved semi-batch system, the adsorption phenomenon was negligible and only dissolution was observed. Thus, the improved semi-batch system is proposed as a more accurate method to predict the risk of mercury elution from flue gas desulfurization gypsums.

Acknowledgments

I would like to express my deep gratitude to my academic advisor Professor Emeritus Katsuyasu SUGAWARA of the Faculty of Engineering Science, Akita University for believing in me, for the patience and for offering endless guidance, support and motivation since my arrival in Japan and enrollment in the graduate school of Engineering and Science in Akita University in September 2016.

Besides my academic advisor, I would also like to express my sincere gratitude to the rest of my dissertation committee members: Professor Hirokazu OKAWA, Professor Kenji MURAKAMI, Professor Sumio KATO and Professor Takayoshi SHINDO, for their great support and invaluable advice in preparing this dissertation.

I would also like to extend my sincere gratitude to Professor Emeritus Takuo SUGAWARA, Faculty of Engineering Science, Akita University for the mentorship, support, valuable scientific and general life lessons and words of encouragement.

I would also like to express my heartfelt appreciation to Professor Takahiro KATO of our laboratory, for giving advice and consistently supporting and kindly answering questions and giving technical assistance at any time. My sincere gratitude also goes to Dr. Kosuke SAKUSABE for his patience in assisting me in how to use most laboratory equipment. And I would also like to thank other laboratory colleagues for helping me out with Japanese language and for helping me to navigate the day-to-day in our laboratory.

In addition, I would like to thank the Japan International Cooperation Agency (JICA) for offering the scholarship through the KiZUNA program which gave me the opportunity to join this graduate school. I gratefully acknowledge the financial support, the support in my daily life since my arrival in Japan. Without they precious support it would not be possible to conduct this research.

Finally, I would like to thank my family and friends for their consistent warm support.

August, 2022

Dorcas L. E. Uaciquete

Peer-Reviews Journal Papers related to this thesis

(1) Dorcas L. E. Uaciquete, Kosuke Sakusabe, Takahiro Kato, Hirokazu Okawa, Katsuyasu Sugawara, Risehiro Nonaka, "Influence of unburned carbon on mercury chemical forms in fly ash produced from a coal-fired power plant", ***Fuel***, 300 (15), 120802 (2021).

(Corresponding to Chapter 3)

(2) Takahiro Kato, Dorcas L. E. Uaciquete, Gai Onodera, Hirokazu Okawa, Katsuyasu Sugawara, Nakorn Worasuwannarak, "Changes in the sulfur forms of subbituminous coals during oxidation with hydrogen peroxide and peracetic acid", ***Fuel***, 330, 125544 (2022)

(Corresponding to Chapter 2)

(3) Dorcas L. E. Uaciquete, Takahiro Kato, Hirokazu Okawa, Katsuyasu Sugawara, Risehiro Nonaka, "Elution behavior of mercury in desulfurization gypsum produced in a coal-fired power plant", ***Fuel***, JFUE-D-22-05395. **(Under review)**

(Corresponding to Chapter 4)

Papers presented at domestic conferences related to this thesis

(1) Dorcas L. E. Uaciquete, Kosuke Sakusabe, Takahiro Kato, Hirokazu Okawa, Katsuyasu Sugawara "Chemical forms of mercury in fly ash from coal-fired power plants"
The 57th Annual Conference on Coal Science (2020, Kagawa, Online) [優秀賞・日本エネルギー学会奨励賞]

(Corresponding to Chapter 3 and 4)

(2) Dorcas L. E. Uaciquete, Takahiro Kato, Hirokazu Okawa, Katsuyasu Sugawara
"Elution behavior of mercury in desulfurized gypsum produced from coal-fired power plants"
The 58th Annual Conference on Coal Science (2021, Sendai, Online)

(Corresponding to Chapter 4)

Papers presented at other conferences

(1) Dorcas L. E. Uaciquete, Takahiro Kato, Hirokazu Okawa, Katsuyasu Sugawara: "Composition and Self-Heating Behavior of Moatize Coals, Moatize Coal Basin, Mozambique"
The 54th Coal Science Conference (2017, Akita)

(2) Dorcas L.E. Uaciquete, Takahiro Kato, Hirokazu Okawa, Katsuyasu Sugawara
"Activated of Carbon Prepared from Mozambican for Heavy Metals Adsorption"
The 55th Coal Science Conference (2018, Kitakyushu)